Applicability of Landsat 8 Thermal Infrared Sensor for Identifying Submarine Groundwater Discharge Springs in the Mediterranean Sea Basin

Sònia Jou-Claus [1,2], Albert Folch [1,2], Jordi Garcia-Orellana [3,4]

[1] Department of Civil and Environmental Engineering, Universitat Politècnica de Catalunya, Jordi Girona 1-3, 08034 Barcelona, Spain
[2] Associated Unit: Hydrogeology Group (UPC-CSIC), Barcelona, Spain
[3] Institut de Ciència i Tecnologia Ambientals – ICTA, Universitat Autònoma de Barcelona, 08193 Bellaterra, Spain
[4] Departament de Física, Universitat Autònoma de Barcelona, 08193 Bellaterra, Spain

Correspondence to: Sònia Jou-Claus (soniajouclaus@gemail.com)

Abstract. Submarine groundwater discharge (SGD) has received increasing attention over the past two decades as a source of nutrients, trace elements, and ocean pollutants that may alter coastal biogeochemical cycles. Assessing submarine groundwater flows and their impacts on coastal marine environments is a difficult task, since it is not easy to identify and measure these water flows discharging into the sea. The aim of this study is to demonstrate the significant usefulness of the freely-available thermal infrared (TIR) imagery of the Landsat 8 thermal infrared sensor (TIRS) as an exploratory tool for identifying SGD springs worldwide, from local to regional scales, for long-term analysis. The use of satellite thermal data as a technique for identifying SGD springs in seawater is based on the identification of thermally-anomalous plumes obtained from the thermal contrasts between groundwater and sea-surface water. In this study we use the TIR remote sensing (TIR-RS) imagery provided by Landsat 8 at a regional scale and discuss the principle limiting factors of using this technique in SGD studies. The study was developed in karstic coastal aquifers in the Mediterranean Sea basin during different seasons and under diverse meteorological conditions. Although this study demonstrates that the freely-available satellite TIR remote sensing is a useful method to identify coastal springs in karst aquifers both locally and regionally, the limiting factors include technical limitations, geological/hydrogeological characteristics, environmental and marine conditions and coastal geomorphology.

1.Introduction

Submarine groundwater discharge (SGD) is an important component of the hydrological cycle and has been commonly defined as any flow of water across the continental margin in the ocean-aquifer interface, regardless of fluid composition or driving force with spatial scale lengths of meters to kilometers (Burnett

Eliminado: to
Eliminado: to the ocean
Eliminado: prove
Eliminado: great
Eliminado: to
Eliminado:
Eliminado: to
Eliminado:
Eliminado: We propose a conceptual framework to apply this technique worldwide and also discuss the limitations of using this technique in SGD studies.
Eliminado: on a regional scale
Eliminado: at
Con formato: Inglés (americano)
Con formato: Normal (Web)
Código de campo cambiado
Con formato: Inglés (americano)

& Dulaiova, 2003; Moore, 2010; Taniguchi et al., 2019). This definition includes meteoric fresh groundwater resulting from inland recharge, but also seawater circulated through the sediments of coastal aquifers (Burnett & Dulaiova, 2003). Both water flows mix in coastal aquifers, where biogeochemical reactions may occur when this groundwater interacts with the geological matrix (Moore, 1999; Moore, 1999; Moosdorf et al., 2021; Rocha et al., 2021; Ruiz-González et al., 2021). This dynamic mixing zone influences the transfer of chemical compounds such as nutrients, trace metals and other contaminants to coastal waters (Alorda-Kleinglass et al., 2019; Boehm et al., 2004; Rodellas et al., 2015; Trezzi et al., 2016). SGD-derived inputs from chemical compounds can highly impact coastal ecosystems, by influencing productivity, biomass, species composition and sonification (Andrisoa et al., 2019; Garcés et al., 2011; Garcia-Orellana et al., 2016; Krest et al., 2000). According to Garcia-Orellana et al., (2021) groundwater discharge pathways of SGD can be grouped into five different SGD pathways according to the characteristics of the processes): 1) Terrestrial groundwater discharge; 2) Density-driven seawater circulation; 3) Seasonal exchange of seawater; 4) Shoreface circulation of seawater and 5) cm-scale porewater exchange (PEX). The discharge of fresh groundwater (Pathway 1) and, to a lesser extent, density-driven seawater circulation (Pathway 2), are the only mechanisms that represents a net source of freshwater, usually mixed with seawater, to the coastal ocean. The SGD discharge process related to this fresher fraction of SGD occurs mainly through three different ways: coastal onshore springs, which discharge on the coastline via surface sinkholes (Garcia-Solsona et al., 2010; Mejías et al., 2012); submarine springs, where the discharge occurs via deep sinkholes (Bakalowicz, 2015; Fleury et al., 2007); and diffuse discharge, a type of discharge which is not concentrated and occurs throughout sediments (Rodellas et al., 2012).

Identifying and mapping groundwater discharge areas is challenging, despite the number of traditional methods available for locating the main groundwater discharge locations and quantifying their flow rates. These methods include simple procedures such as deploying traditional local knowledge, conducting visual observation, monitoring changes in vegetation as well as in water temperature and salinity, and using seepage meters or radioactive isotope tracers (Garcia-Orellana et al., 2021; Mejías et al., 2012; Rosenberry et al., 2020; Schubert et al., 2014). Apart from these methods, several authors have suggested Thermal Infrared Remote Sensing (TIR-RS) as an alternative methodology for identifying potential SGD spring sites, since it enables the screening and study of inaccessible zones and/or areas with a scaracity of hydrogeological information (Wilson & Rocha, 2012). Temperature has been used successfully to study SGD by comparing the relatively constant temperature of groundwater with that of surface seawaters, which fluctuates seasonally (Dale & Miller, 2007). In general, groundwater maintains a relatively constant temperature between depths of 5 m and 100 , approximately 1 - 2 ºC higher than the mean annual air temperature (Anderson, 2005). The detection of SGD springs via TIR-RS is possible in any environment where there is thermal contrast between the discharging fluid and the receiving surface water body (Kelly et al., 2013). TIR images have the potential to identify the location of major SGD springs, as well as to study their spatial variability, by exploring the temperature difference between coastal seawater and brackish groundwater discharges.

There are two types of platforms for obtaining thermal infrared information: airborne TIR-RS (airplane, helicopter and drone), and satellite TIR-RS (Modis, Aster, Landsat). Airborne TIR has been used for

Con formato: Inglés (americano)
Código de campo cambiado
Con formato: Inglés (americano)
Eliminado:)
Código de campo cambiado
Con formato: Inglés (americano)
Eliminado: of
Código de campo cambiado
Eliminado: ¶
Código de campo cambiado
Con formato: Inglés (americano)
Con formato: Inglés (americano)
Eliminado: Depending on its geological background SGD occurs in three different ways: coastal onshore springs (Garcia-Solsona et al., 2010; Mejías et al., 2012), diffuse submarine springs (Rodellas et al., 2012) and focused submarine springs (Bakalowicz, 2015; Fleury et al., 2007; Katz et al., 2009; Yobbi, 1992).¶
Eliminado: to
Eliminado: e
Eliminado: easy
Eliminado: , changes
Eliminado:
Eliminado: (Mejías et al., 2012; Schubert et al., 2014)
Eliminado: to
Eliminado: that have
Eliminado: ce
Eliminado: using
Eliminado:
Eliminado: m depth
Con formato: Fuente: TimesNewRomanPSMT
Eliminado: to

different applications; for example Shaban et al. (2005) and Akawwi et al., (2008), conducting aerial TIR surveys along the Mediterranean and Dead Sea coastlines to identify potential SGD sites. Kelly et al. (2013) used TIRS images from localized point-source SGD to demonstrate that groundwater plume areas are linearly and highly correlated to in-situ groundwater fluxes. Airborne TIR-RS has also been applied in combination with other methods, not only for qualitative SGD recognition, but also for quantifying groundwater flows from freshwater springs (Danielescu et al., 2009; Mejías et al., 2012). In the coastal carbonate aquifer of El Maestrazgo (Iberian Peninsula), a combination of complementary techniques was used to locate submarine springs via airborne high-resolution thermal infrared, radon measurements and physical-chemical anomalies and to quantify the groundwater discharge by direct quantification with flowmeters and Ra isotopes (Mejías et al., 2012). Tamborski et al. (2015) combined airborne TIR overflights with coastal radionuclide surveys to investigate the significance of SGD along the north shore of Long Island (NY, US) to provide quantitative evidence for TIR-RS as a tool to remotely identify and measure SGD. Finally, Danilescu et al. (2009) assessed total freshwater discharge in two small nutrient-sensitive estuaries in Prince Edward Island (Canada) using a combination of TIR images, direct discharge measurements and numerical simulations.

Compared to airplane, helicopter and drone platforms, satellite TIR-RS has some characteristics that limit its use for coastal water observation. The temporal resolution is fixed and varies depending on the satellite, with a minimum daily revisit frequency and a maximum frequency of every 16 days for a specific area. Furthermore, the spatial resolution, which varies between 30 and 1000 meters, is lower than airborne resolution. This results in the fact that small thermal anomalies, induced by small flows of SGD, are likely not to be detected. Additionally, satellite TIRS images are affected by atmospheric conditions (i.e., clouds and shadows). However, satellite TIR-RS imagery has the great advantages of being free of charge (Landsat), easily accessible, globally available, multi-temporal, and covering a regional scale instantaneously. These advantages turn satellite TIR-based approaches into a viable and promising option for detecting SGD worldwide.

There are several satellite missions capable of measuring sea surface temperatures (SST) with a moderate spatial resolution and acquisition: Advanced Spaceborne Thermal Emission and Reflection Radiometer (ASTER), and the Landsat satellite among others, which provide appropriate spatial and temporal resolution for large-scale SGD monitoring. For those sensors suitable for SGD research, Landsat is the one with the longest TIR data provision (from 1982 until today and already planned to go beyond 2030 (Wulder et al., 2019)) and the one most widely applied for the purposes of SGD research (Wilson and Rocha, 2012, among others)

The use of satellite imagery in SGD studies has evolved in parallel with the launch of new sensors that feature spatial resolution improvements over previous sensors. However, the application of satellite TIR images is neither extensive nor widespread compared to the airborne TIR images. Several SGD studies used Landsat 7 to locate groundwater discharge areas (e.g. Wang et al., 2008), to detect known but previously unmapped SGD locations (Varma et al., 2010), to determine the spatial extent and scale of SGD-derived temperature anomalies (Wilson & Rocha, 2012), and to infer a SGD temporal variation using long-term thermal anomaly size variations (Mallast et al., 2014). More recent studies used data

Eliminado:
Eliminado: also
Eliminado: i
Eliminado: with
Eliminado: i
Eliminado: y
Eliminado: ,
Eliminado: to
Eliminado: satellite
Eliminado: ly
Eliminado: (Mejías et al., 2014;
Eliminado: ¶
Eliminado:
Eliminado: ,
Eliminado: ,
Eliminado: ,

obtained by Landsat 8 TIRS to identify and characterize SGD sites using the sensors technical improvements. For example, McCaul et al. (2016) proposed a multiapproach methodology for understanding submarine and intertidal groundwater discharge patterns. Xing et al. (2016) evaluated the capability of satellite remote sensing methods (Landsat 7 and 8) to detect thermal anomalies related to SGD as a possible index of the presence of offshore low-salinity groundwater storage at local scale. To the best of our knowledge, there is no study that thoroughly compares SGD locations with satellite-data-derived thermal anomalies over large spatial scales in order to assess the suitability of satellite TIR-RS data in conducting SGD research.

The aim of this work is to study the usefulness of satellite TIR images at different sites, covering a large scale and in different seasons to assess whether Landsat 8 TIR-RS can be used as an exploratory tool for identifying SGD springs worldwide, from local to regional scales, for long-term analysis. The second aim is to discuss the influencing factors to be considered in the identification of SGD at the local and regional level.

The study was carried out on the coastal karstic aquifers of the Mediterranean Sea basin, where there are many local studies that describe the discharge processes thanks to the significant connectivity between this coastal aquifer type and the sea (Bakalowicz, 2005; Barberá and Andreo, 2015; Worthington, 1999). In this hydrogeological context, SGD takes place mainly through submarine or aerial springs (point source). Although groundwater discharge from submarine springs represents a negligible fraction of the global SGD (Luijendijk et al., 2020), in some areas, such as the Mediterranean Sea, this fraction can be locally important, strongly influencing marine ecosystems and serving as a freshwater resource for the population (Rodellas et al., 2015; Alorda-Kleinglass et al., 2021). To validate the temporal effectiveness of this technique, Landsat-8 images from 2017 and 2018 on the coasts of the Mediterranean Sea basin were used to locate SGD springs previously described in the scientific literature, showing in which period of the year these SGD springs are observable via satellite. In addition, we will hypothesize and discuss those factors that may condition the identification of SGD springs in order that future studies might take them into account when using satellite remote sensing TIR techniques.

2. Methods

2.1. Study area

The Mediterranean basin has been selected for this study because it is one of the areas of the world where numerous SGD studies have been carried out and where dozens of coastal springs have been described dating back to ancient times in countries such as Spain, France, Italy, Croatia, Greece, Turkey, Syria, Lebanon and Libya (Figure 1). In this study, we focus on a set of 54 springs mentioned in the scientific peer review literature published in English (Bakalowicz, 2018; Basterretxea et al., 2010; Fleury et al., 2007; Mejías et al., 2012 and Garcia-Solsona et al., 2010) where groundwater discharge is known to occur and there is a description of the hydrogeological context of each spring (Supplementary Material 1). The

Eliminado: s'
Eliminado: to
Eliminado: To the best of our knowledge, there is not a single study that thoroughly compares known SGD locations to satellite-data derived thermal anomaly indications over larger spatial scales, to analyze the appropriateness of satellite TIR-RS data for SGD research in a statistically robust manner.¶
Con formato: Sin Resaltar
Eliminado: study
Eliminado: prove
Eliminado: great
Eliminado: in
Eliminado: at
Eliminado: to
Con formato: Fuente: (Predeterminada) +Cuerpo (Times New Roman), 12 pto, Sin Cursiva, Color de fuente: Color personalizado(RGB(38,50,56)), Diseño: Claro (Blanco)
Eliminado: The second aim is to define a conceptual application framework, identifying and discussing the principal limitations of satellite TIR-RS in the study of SGD at the local and regional level.¶ ¶
Eliminado: due
Eliminado: great
Eliminado: water
Eliminado: (Rodellas et al., 2015; Moosdorf & Oehler, 2017). To validate the temporal effectiveness of this technique, Landsat-8 images from 2017 and 2018 on the coasts of the Mediterranean Sea basin were used to locate SGD springs described previously in the literature, showing at what period of the year and under what hydrogeological, marine and environmental conditions these SGD springs are observable with a satellite.¶

number of springs included in the study represents at least 88% of the submarine karst springs described in the English peer review literature concerning Mediterranean basin.

The SGD contribution to the Mediterranean ranges from 3 to 50·10^{11} $m^3 \cdot yr^{-1}$, where fresh groundwater inputs represent 1 – 25% of the total SGD inputs (Rodellas et al., 2015). SGD has been described and studied in several locations along the Mediterranean coast (e.g., Bakalowicz, 2015; Mejías et al., 2012; Tulipano et al., 2005; Bejannin et al., 2017). The Mediterranean basin is characterized by 46% of its coastline being formed by karstic aquifers (Bakalowicz, 2015; Fleury et al., 2007; Trezzi et al., 2016). Its narrow continental shelves prevent large tidal amplification along the coast; tidal amplitude is usually less than 0.2 m (Werner et al., 2013). The Mediterranean climate is seasonal, characterized by windy, mild, wet winters and by relatively calm, warm and dry summers. Strong local winds, such as the cold and dry Tramontana, Mistral and Bora, from the north, and the hot and dry Sirocco, from the south, are typical of the region. These strong regional and seasonal wind regimes provide a substantial amount of vertical mixing in the seawater column (GROUP, 1970). In general, the main rainfall season is during fall and spring, with an average annual precipitation of 500 mm y^{-1} (Andreo & Carrasco, 1993). The sea temperature is approximately between 26 - 30 and 14 - 19 ºC in the summer and winter, respectively.

The available information for each of the 54 studied springs (Supplementary Material 1) shows that the mean flow rates range between 0.009 and 50 $m^3 \cdot s^{-1}$, the distances from the shore range from the coastline to 1 km offshore, and that discharge depths vary between 7 m.a.s.l and 150 m.b.s.l. In accordance with these characteristics, we might classify the studied springs in 5 groups. The first group of springs discharge inland near the seashore and reach the sea through small streams; these karstic springs are located between 300 and 500 m inland and at elevations of 2, 3 and 15 m.a.s.l for Patan in Croatia, Almyros of Iraklio in Greece and Maro in Spain, respectively. The second group of springs discharges in coastal lagoons at a distance of 100 m from the sea shore and a depth of 4 m.b.s.l (Font Dame and Font Estramar in Salses-Laucate lagoon in France), and at an unknown shore distance and 30 m.b.s.l (Vise in Thau lagoon respectively). The third group of springs is located between 0 and 10 m from the shoreline and in shallow sea waters of between 0 and 7 m.b.s.l (Torre Badum, Las Fuentes, Font de Dins in Spain, Ain Zayana in Libya, Agios Nikolaos, Cephalonia and Anavalos Kiveri in Greece and Ovacik and Gokova in Turkey). The fourth group of springs is also located close to the shoreline, but at a water column depth of 12 m.b.s.l. The two springs of this group are Moraig in Spain and Port Miou and Bestouan in France. The fifth and last group consists of Mortola in Italy and Chekka in Lebanon, in which discharges occurs offshore between 100 m and 1 km and with a water column depth of between 35 and 150 m.b.s.l.

The type of coastal karst aquifer studied has been defined using the same classification as in Tulipano et al. (2005) for Mediterranean coastal karst aquifers. The first type are systems with poorly-developed, but highly-fractured karstification. This karst type included 3 different subsystems in which 1) faults dissect the aquifer such as in the Gokova (4 springs) (Bayari & Kurttas, 2002) and Ovacik spring, where the faults are located in the underlying beds that extend towards the sea (Elhatip, 2003); 2) groundwater flows along the zones of cracks, fractures and karst hollows, such as in the Donnalucata spring (Povinec et al., 2006); and 3) groundwater flows through stratification joints, such as in the Mortola spring (Fleury et al., 2007). The second type are systems with well-developed karstification connected to the sea (e.g., Moraig,

Eliminado: (
Eliminado: –
Eliminado:)
Eliminado: ;
Eliminado: t
Eliminado: 18
Eliminado: 27
Eliminado: 7

Port Miou, Bestouan, Almyros of Iraklio, Almiros of Agios Nikolaos, Cephalonia, Ain Zayana and Chekka). The last type of defined karst system is a well-developed karstification but with low connectivity with the sea. This group is represented by only two springs: Kiveri Anavalos in Greece and Vise in France.

2.2. Landsat 8 TIRS data acquisition

To determine the optimal time period for SGD detection using remote sensing, the SST of a series of images covering all seasons was compared. The TIRS instrument of Landsat 8 is a thermal imager with two thermal infrared bands centered at 10.8 µm and 12.0 µm and a ground sampling distance (GSD) of 100 m. However, all thermal images are resampled using a cubic convolution to 30 m (Roy et al., 2014). To carry out this study, only the thermal band 10 TIRS 1 (10.6 - 11.2 µm) of the 11 Landsat 8 bands was used to study the SGD sites. The other Landsat 8 thermal band, 11 TIRS 2 (11.50 - 12.51 µm), was not used because the data collected in this band had some large calibration uncertainties (U.S. Geological Survey, 2014b).

A total of 27 path/row combinations were analyzed with the Landsat 8 TIR images of the Mediterranean coast between January 2017 and December 2018 to cover all 54 known SGD sites. To that end, a total of 1296 images (2 images per month for the two years of study) were acquired from the U.S. Geological Survey (USGS) with cloud coverage between 0% and 90% in each image. A manual inspection of all images resulted in finer selection of 365 images with cloud-free conditions above the areas of interest (Supplementary Material 2). The finer selection of cloud-free images were used for subsequent steps.

2.3. Deriving SST values from Landsat 8 TIRS data

Data processing included the conversion of digital numbers to SST, including an atmospheric correction of each image following the methodology presented by Chander et al. (2009). Image processing began with radiometric correction, which was performed by converting the digital number (DN) to sensor spectral radiance through band-specific rescaling gain and bias factors according to Equation (1).

$$L\lambda = G_{rescale} * Q_{cal} + B_{rescale} \quad (1)$$

where L_λ is the sensor spectral radiance [$W \cdot m^{-2} \cdot sr^{-1} \cdot \mu m^{-1}$]; $G_{rescale}$ is the band-specific rescaling gain factor [$W \cdot m^{-2} \cdot sr^{-1} \cdot \mu m^{-1} \cdot DN^{-1}$]; Q_{cal} is the quantized and calibrated standard product pixel values (DN) and $B_{rescale}$ is the band-specific rescaling bias factor [$W \cdot m^{-2} \cdot sr^{-1} \cdot \mu m^{-1}$].

The next step was an atmospheric correction to remove the atmospheric component of the recorded thermal signal which strongly depends on atmospheric conditions (aerosol content, humidity, temperature etc.) at a specific recording time and place. To atmospherically correct images at sensor spectral radiance, it was necessary to transform them into surface radiance of an ideal 'black body', considering the scene-

Eliminado: In this study, we selected 54 springs located in the Mediterranean Sea basin (Supplementary material 1) based on published scientific literature (Bakalowicz, 2018; Basterretxea et al., 2010; Fleury et al., 2007; Mejías et al., 2012) where groundwater discharge is known to take place and the hydrogeological context has been previously described. These springs are located in Spain, France, Italy, Croatia, Greece, Turkey, Syria, Lebanon and Libya (Figure 1).¶
The mean flow rates of the studied springs range between 0.009 and 50 $m^3 \cdot s^{-1}$. The depth and/or elevation of the discharge area with respect to sea level ranges from -30 m to 9 m. The distance of the discharge ranges between 0 and 3000 m from the shoreline. The type of coastal karst aquifer has been defined using the same classification as in Tulipano et al. (2005) for Mediterranean coastal karst aquifers. The classification includes three types: (1) systems with poorly-developed, but highly fractured karstification; (2) systems with well-developed karstification below sea level and open to the sea and (3) systems with well-developed karstification below sea level, partially or totally closed to the sea.¶

Eliminado: Only band 10 has been used to study temperature differences in water to detect SGD sites, because data collected in band 11 of the TIRS has some large calibration uncertainties (U.S. Geological Survey, 2014b).¶

Eliminado: 5

Eliminado: To that end, a total of 1536 images

Eliminado: ¶

Eliminado: ¶

Con formato: Inglés (americano)

Con formato: Inglés (americano)

Con formato: Inglés (americano)

Eliminado: [$W \cdot (m^{-2} \cdot sr^{-1} \cdot \mu m^{-1})$]

Con formato: Inglés (americano)

Con formato: Espacio Antes: 0 pto

Con formato: Inglés (americano)

Eliminado: [$(W \cdot (m^{-2} \cdot sr^{-1} \cdot \mu m^{-1}) \cdot DN^{-1}$]

Con formato: Inglés (americano)

Con formato: Inglés (americano)

Con formato: Fuente: TimesNewRomanPSMT, Inglés (americano)

Eliminado: [$W \cdot (m^{-2} \cdot sr^{-1} \cdot \mu m^{-1})$]¶
¶

Con formato: Inglés (americano)

Con formato: Normal (Web)

Con formato: Inglés (americano)

Con formato: Fuente: TimesNewRomanPSMT, Inglés (americano)

specific up- and down- welling radiance and transmission values and the emissivity of the water surface, according to Equation (2) (Barsi et al., 2003).

$$L_t = \frac{L_\lambda - L_U - \tau * (1-\varepsilon) * L_D}{\tau * \varepsilon} \quad (2)$$

where L_t is the radiance of an ideal 'black body' [$W \cdot m^{-2} \cdot sr^{-1} \cdot \mu m^{-1}$]; L_λ is the sensor spectral radiance [$W \cdot m^{-2} \cdot sr^{-1} \cdot \mu m^{-1}$]; L_U is the upwelling radiance [$W \cdot (m^{-2} \cdot sr^{-1} \cdot \mu m^{-1})$]; L_D is the downwelling radiance [$W \cdot m^{-2} \cdot sr^{-1} \cdot \mu m^{-1}$]; ε is the emissivity of the surface [-] and τ is the atmospheric transmission [-].

A web-based atmospheric correction tool (Atmospheric Correction Parameter Calculator) developed by Barsi et al. (2003) based on MODTRAN was used to obtain values for atmospheric transmissivity and the upwelling and downwelling radiances of the atmosphere. The emissivity of water in the Landsat 8 TIR bands ranges from 0.98 (band 11) to 0.99 (band 10) and in this study, we assume a constant emissivity of 0.99 (Wen-Yao et al., 1987).

Finally, to obtain the sea surface temperature (SST), the corrected radiances were introduced into Equation (3).

$$T = \frac{K_2}{\ln\left(\frac{K_1}{L_t} + 1\right)} \quad (3)$$

where T is the effective sensor brightness temperature [K]; L_t is the radiance of an ideal 'black body' [$W \cdot m^{-2} \cdot sr^{-1} \cdot \mu m^{-1}$]; K_1 is prelaunch calibration constant 1 [$W \cdot m^{-2} \cdot sr^{-1} \cdot \mu m^{-1}$]; and K_2 is prelaunch calibration constant 2 [ºK].

The resulting atmospherically-corrected SST data represents temperature with an error of less than 1.3 ºK for the temperature range 270 - 330 ºK. This temperature represents the skin temperature of the water (<1 mm of the upper most water layer), which differs from the bulk temperature below it by about 0.1 ºK due to sensible heat fluxes, evaporative heat loss, and long wave radiation (Donlon et al., 2002; Wloczyk et al., 2006).

2.4 Site inter-comparison between single image and multiple images

Temperature maps of coastal waters were created from temperature data to assess the significance of the SST anomalies. The identification of SGD spring sites was based on the assumption that temperatures of discharging groundwater may be different than seawater and less variable than seawater temperatures

Eliminado: earth's surface

Eliminado: ¶
Con formato ... [1]
Con formato: Normal (Web), Izquierda
Eliminado: [W·(m-2 · sr-1 · µm-1)]
Con formato ... [2]
Eliminado:
Con formato: Inglés (americano)
Eliminado: [W·(m-2 · sr-1 · µm-1)]
Con formato ... [3]
Eliminado: [W·(m-2 · sr-1 · µm-1)]
Con formato ... [4]
Eliminado: The applied value for water emissivity in band 10 was 0.9904 (Wen-Yao et al., 1987).¶

Eliminado: ¶
Con formato ... [5]
Con formato: Espacio Antes: 0 pto
Eliminado: [W·(m-2 · sr-1 · µm-1)]
Con formato ... [6]
Eliminado: [W·(m-2 · sr-1 · µm-1)]
Con formato: Inglés (americano)
Eliminado:
Con formato ... [7]
Eliminado: [K].¶
¶
Con formato: Inglés (americano)
Con formato: Normal (Web), Izquierda
Con formato ... [8]
Eliminado: … for the temperature range of ... [9]
Con formato: Inglés (americano)
Código de campo cambiado
Con formato ... [10]

throughout the year. SGD spring sites were analyzed using two different procedures. First, single images were used to identify SGD springs by means of the water temperature anomalies. As a second step of the single image approach, the change between images along the study period was also evaluated. This qualitative analysis allows us to observe variations in the morphology and temperature range of the known discharge plume between images. As a second approach, called multiple imaging, SGD spring sites were detected by evaluating the pixel-by-pixel standard deviation (SD) across all image sets. Lower values of SD were used as indicators for groundwater discharge using sea surface temperature (SST) data series. This statistical parameter has been previously applied in semi-arid areas to study groundwater and surface water interactions and identify spring discharge into lakes or enclosed seas (Mallast et al., 2014; Tcherepanov et al., 2005). It was assumed that groundwater tends to be less variable than surface water, which varies seasonally and daily. The applied multi-temporal thermal remote sensing approach was based on a variable number of Landsat 8 TIRS images. The images used to calculate the standard deviation varied between 5 and 17 images, depending on the number of images without clouds available for each studied site. The resulting thermal maps were combined with satellite imagery from Google Earth (only the land part) using GIS (QGIS Las Palmas) to show the location the SGD springs at the identified sites.

Eliminado: This analysis allowed identifying variations in the morphology of the discharge plume

Eliminado: between

3. Results and discussion

Eliminado: The thermal mapping results were combined with orthophoto maps (only the land part) within a GIS to locate the SGD springs at the identified sites.¶
¶

3.1 Overall identifications

As an example of the Landsat 8 TIR images analyzed in the Mediterranean Sea basin, the thermal images of the Almyros SGD spring in Agios Nikolaos (Crete, Greece) throughout the year 2017 are shown in Figure 2. In general, a thermal anomaly plume is observed in several of the 23 images (one of the July images is missing) occurring near and perpendicular to the coastline, reflecting the continuous discharge of groundwater. Since a satellite image provides the sea surface temperature (SST) of the first millimeter of seawater (Donlon et al., 2002; Wloczyk et al., 2006), the thermal contrast due to SGD can be observed as the fresh groundwater flows over seawater due to its lower density (i.e., lower salinity) (Wilson & Rocha, 2012). The images series of Almyros Agios Nikolaos (Figure 2) shows how thermal contrast caused by the groundwater discharge cannot be observed throughout the whole year. The thermal contrast is more identifiable from the second half of April until the end of October, but the best thermal plume observations were from June to October (Figure 2). Conversely, this spring cannot be identified from November to March. The groundwater discharge was not identified in February and December due to the absence of thermal contrast, and in the other months (January, March and November) because clouds made identification difficult. Thus, the overall percentage of time for optimal SGD spring identification was 37% in 2017.

Eliminado: the thermal contrast is because the groundwater is located above the seawater because of its lower density due to its different temperature and salinity (Wilson & Rocha, 2012). ¶

Eliminado: .5

If the same approach is applied for the total of 54 SGD springs studied, only 23 springs were identified in individual images, representing a 44% success rate for the technique over the entire study period (2017 and 2018). The success percentage for identifying the 23 SGD springs according to the period of the year, is shown in Supplementary Material 3. The highest success percentage for SGD identification was during the summer, specifically from June to September (Figure 3), which corresponds to an average of 21% of

Eliminado: .4

Eliminado: of

Eliminado: s

Eliminado: m

Eliminado: 2

the images analyzed. Conversely, the SGD springs were not identified in the remaining 79% of the images. The winter period, from December to February (Figure 3), had the lowest percentage of SGD spring identifications.

3.2 Influencing factors to consider in the identification of SGD springs

The analysis of the images of the Mediterranean coast obtained by Landsat 8 TIRS during 2017 and 2018 was successful for several studied springs but did not identify SGD springs in all the images analyzed. Thus, identifying SGD springs using Landsat 8 TIRS has some limitations, as the success rate was slightly less than 50%. The following potential limitations have been previously reported in the literature in some local studied areas: only information for the first millimeters of seawater is available (Donlon et al., 2002; Wloczyk et al., 2006); spatial resolution (Wilson & Rocha, 2012); period of the year (Bayari & Kurttas 2002; Wilson & Rocha 2012; Xing et al., 2016); the results are highly dependent on atmospheric temperature, seawater currents, wind speed and direction, sea surface effects (Kelly et al., 2013) and cloud cover; and the need for specialist knowledge to convert the data into accessible (visualized) information (McCaul, 2016).

Given the above-mentioned limitations, we propose a conceptual framework of factors representing technical limitations in order to asses those issues that should be considered when applying TIR-RS to the study of SGD. These technical limitation factors can be grouped as follows: (1) technical limitations, (2) geological/hydrogeological characteristics, (3) environmental and marine conditions, (4) coastal geomorphology and (5) anthropogenic sources (Figure 4).

3.2.1 Technical limitation factors

Some of the main limitations of the technique are related to the temporality of obtaining images, the spatial resolution, the availability of images in the desired period and the atmospheric conditions during the image capture. Each satellite has an image acquisition spatial and temporal resolution, and therefore the results are subject to these pre-established conditions. For Landsat 8 TIRS, the temporal resolution is two weeks, and the spatial resolution is 100 m resampled to 30 m, so a smaller thermal anomaly plume than this produced by an SGD spring will not be identified. For example, in the 20 m wide semi-enclosed cove of Alcalfar (Menorca, western Mediterranean) there are several described springs (García-Solsona et al., 2010) that were not identified by satellite due to the small dimensions of the cove (García-Solsona et al., 2010). The availability of satellite images depends, in some cases, on technical problems that the satellite experiences during image collection, which implies that there are annual series of images with some missing images. In the example used in Figure 2, where the Almyros of Agios Nikolaos (Greece) SGD spring is identified, only 23 of the 24 images that should have been produced during 2017 were obtained. The striping noise that it can be seen in the images (Figure 2) and which affect TIR bands especially is another technical limitation. Sometimes the difference is so large that it would hinder a proper SGD detection (Gerace and Montanaro, 2017).

Eliminado: 3.2 Conceptual framework to asses factors influencing the identification of SGD springs ¶
Eliminado: with
Eliminado: ,
Eliminado: ,
Eliminado: ,
Eliminado: ,
Eliminado: Given the limitations, we propose a conceptual framework to assess the following types of factors that should be considered: (1) technical limitations, (2) geological/hydrogeological characteristics, (3) environmental and marine conditions, (4) coastal geomorphology and (5) anthropogenic sources (Figure 4). ¶
Eliminado: ,
Eliminado: capture
Eliminado: In the Mediterranean basin, the Alcalfar spring in Menorca (Spain) (Garcia-Solsona et al., 2010), which discharges in a semi-enclosed area with an approximate width of 20 meters, was not identified.
Eliminado: to identify the Almyros of Agios Nikolaos

Other important limitations related to the technique include the atmospheric conditions at the time of the image capture. Clouds and clouds shadows change radiometric information leaving the sea surface and prevent a correct analysis of the images. For the Mediterranean Sea basin, of the 80% of the images in which SGD springs were not identified, 60% were due to the high presence of clouds. Thus, clouds are the main factor limiting the identification of SGD springs. The presence of clouds is higher in winter than in summer; therefore, warmer months are much better for identifying SGD springs in the Mediterranean Sea. However, in at least 20% of the cloudless images, it was not possible to observe and locate SGD springs described in the literature. Therefore, a detailed analysis of the cloudless imagery is necessary to confirm the optimal conditions for locating SGD springs in the area of interest (Anderson, 2005).

Eliminado: when
Eliminado: s
Eliminado: are
Eliminado: d
Eliminado: ¶

3.2.2 Geology and hydrogeology limitation factors

The characteristics of coastal aquifers and the different driving forces that allow groundwater discharge into the sea are other factors that can limit the identification of SGD springs. According to Garcia-Orellana (2021), SGD is the combination of fresh terrestrial groundwater discharge driven by hydraulic gradient between land and sea and saline groundwater discharge from the seawater recirculation through the coastal and continental margin. Thus, the thermal signal of both types of groundwater will define the intensity and shape of the plume that can be observed in the sea.

Eliminado: According to Taniguchi et al. (2002), SGD is the combination of fresh groundwater discharge from the land

For coastal aquifer SGD springs, geological factors such as the lithology (e.g., type of rock, degree of karstification, presence of faults or fractures, etc.) determine the hydraulic properties that greatly influence the groundwater flow that discharges into the sea (Sander at al., 1996; Brunner et al., 2007; Edet et al., 1998). Another aspect to consider is the connectivity of the aquifer with the sea. Coastal aquifers may be totally or partially hydraulically connected to the sea, depending on several factors such as the geological structure of the aquifer and the seabed, as well as the hydraulic properties of both onshore and offshore geological formations. In addition, the amount of SGD into the sea depends on the aquifer water budget, which produces variations in groundwater discharge flow. The main factors that influence this budget are the natural variations in recharge at different temporal scales (rainfall events, seasonality, inter-annual changes) and the abstraction of groundwater, which can reduce the discharge of the fresh groundwater component of the SGD, or even induce seawater intrusion into the coastal aquifer. Unfortunately, these factors are linked since in most cases when recharge is low, abstractions tend to be higher.

Eliminado: ¶

In the presented research, from the 54 karstic SGD studied springs, information on the type of coastal karst aquifer is only available for 37% of the springs (Supplementary Material 4). From those, the first karst type system, characterized by poorly-developed but highly-fractured karstification, represents 11% of the springs and 7% of the total where successfully identified. The second type of karst system, characterized by well-developed karstification connected to the sea, represents 22% of the springs, and half of those were identified (11% of the total). Finally, the third karst type system with well-developed karstification but low connectivity with the sea, represent only 4% of the springs, and half of those were identified (1.8% of the total). Therefore, the best geological and hydrogeological settings for identifying

SGD springs are karst systems with well-developed karstification and that are well-connected to the sea, as well as those systems with poorly-developed but highly-fractured karstification. This is because these systems have high transmissivities that can induce high local SGD rates, making it easy to detect their thermal plumes. However, it depends on the recharge area and its rate.

Conversely, low groundwater discharge water volumes may limit the identification of thermal anomalies because they could attenuate the thermal anomaly produced by the SGD. Therefore, low discharge water volumes are unlikely to be identified using this technique. Of the 54 karstic SGD studied springs, the flow rate information was only available for 59% of the springs (Supplementary Material 4). Springs with a flow rate lower than 10 $m^3 \cdot s^{-1}$ represent 40% of the springs. From those, only 50% were identified. The springs with a flow rate higher than 10 $m^3 \cdot s^{-1}$ represent 15% of the springs, and from those 60% were identified. This indicates that apart from flow rate, other factors affect the failure to identify these SGD springs on the coastline.

Inter-annual and annual changes, such as humid-dry periods/seasons, prolonged alteration to the groundwater systems (overexploitation) and extreme events such as strong rainfall storms, etc., can also modify SGD flows. Thus, the research period in which the images were collected is also important because seasonal variations (Lee et al., 2016) can lead to SGD thermal plume variations, not only due to the temperature difference between groundwater and seawater (Lee et al., 2016), but also annual SGD flow rate variations (Michael et al., 2005) that allow their identification.

Regarding hydrogeological conditions in the Mediterranean Sea basin, it was expected that the best seasons for identifying SGD springs using satellite TIR-RS would be spring and autumn, when rainfall is higher and therefore a higher discharge flow rate is expected. However, summer was the best season for identifying SGD springs, indicating that other factors influence the identification of SGD springs using this technique.

3.2.3 Environmental and marine conditions

Other aspects that could affect the thermal contrast between the groundwater plume and the seawater include environmental and marine conditions. Both factors can make the identification of SGD difficult, because they cause seawater mixing with the discharging groundwater, reducing the thermal contrast between them and modifying the sea surface temperature. The main environmental condition that can affect SGD identification is the action of wind, which can mix the first millimeters of the sea surface water, limiting the identification of SGD springs using remote sensing techniques. Similarly, marine conditions can affect SGD identification if they reduce the thermal contrast between the groundwater plume and the seawater. These marine conditions are basically reduced to the coastal water hydrodynamic conditions that can be affected by processes such as the influence of tides or coastal currents, the formation of a pycnocline in surface seawater or the fetch due to wind action. Tides, coastal currents and fetch generate seawater movement and mix groundwater with seawater, causing a thermal contrast attenuation. Similarly, the presence of a pycnocline can result in less vertical mixing of the water column. In subtropical areas with cold winters and hot summers, such as the Mediterranean Sea, coastal waters often

Eliminado: The present study was performed in a specific geological context - coastal limestone with different levels of karstification - with SGD occurring through springs (point source discharge). To analyze the influence of geological and hydrological component on the 54 studied karstic SGD springs, hydrogeological characteristics were analyzed only when detailed information was available, that is, for 33 springs representing 62% of the total (Supplementary material 1). According to the hydrogeological characteristics, 15% of the springs correspond to a karstic system characterized by well-developed karstification connected to the sea (e.g., Moraig, Port Miou, Bestouan, Almyros of Iraklio, Almiros of Agios Nikolaos, Cephalonia, Ain Zayana and Chekka). Of these well-developed springs, most were identified; only the Ain Zayana and Chekka springs were not observed. 9% of the springs 9% of the springs for which karst type information was available, were systems with poorly-developed but highly fractured karstification. These karst systems included 3 different fractured systems in which 1) faults dissect the aquifer such as in the Gokova (4 springs) (Bayari & Kurttas, 2002) and Ovacik spring, where the faults are located in the underlying beds that extend towards the sea (Elhatip, 2003); 2) groundwater flows along the zones of cracks, fractures and karst hollows, such as in the Donnalucata spring (Povinec et al., 2006); and 3) groundwater flows through stratification joints, such as in the Mortola spring (Fleury et al., 2007). Of all these types of SGD spring located in fractured systems, thermal anomalies were only identified in the first type, in which the faults dissect the aquifer. The last type of defined karst system is one with well-developed karstification but low connectivity with the sea. This group is represented by only two springs: Kiveri Anavalos in Greece and Vise in France, of which only the first was identified. Therefore, the best geological and hydrogeological settings for identifying SGD springs are karst systems with well-developed karstification and that are well-connected to the sea, as well as those systems with poorly-developed but highly fractured karstification. This is because these systems can drain large areas of recharge; therefore, SGD springs often have high flow rates, making it is easy to detect their thermal plumes. ¶

¶

SGD spring identification can also be limited by the groundwater flow rate, because the thermal anomaly generating the SGD thermal plume may by generated by the head transported by fresh groundwater flow (convection) and/or by the offshore movement of seawater intrusion (due to conduction and/or convection), which is also affected by groundwater flow rate. Therefore, low discharge water volumes it is unlikely be identified using this technique. In the studied case of the Mediterranean Sea basin, the identified springs have an average flow rate between 0.75 $m^3 \cdot s^{-1}$ and 50 $m^3 \cdot s^{-1}$. The identified springs with high flow rates were Almyros of Iraklio in Greece (with values between 2 and 30 $m^3 \cdot s^{-1}$) and Jurjevska in Croatia (with values between 0.8 – 50 $m^3 \cdot s^{-1}$). The identified SGD springs with low flow rates were Ovacik in Turkey (with values of 0.75 $m^3 \cdot s^{-1}$), Gokova in Turkey (with values between 0.02 - 0.10 $m^3 \cdot s^{-1}$), las Fuentes in Spain (between 0.03-0.17 $m^3 \cdot s^{-1}$) and Moraig in Spain (between 0.3 – 9.0 $m^3 \cdot s^{-1}$). However, there were springs with high flow rates, such as the Ses Ufanes spring in Spain (with values between 20 - 30 $m^3 \cdot s^{-1}$), and Font Dame-Font Estramar (with values between 1 - 15 $m^3 \cdot s^{-1}$), that were not identified, indicating that other factors affect the failure to identify these springs.¶

develop a pycnocline during the summer months, as high temperatures increase the evaporation of seawater, generating an increase in salinity and therefore water density. This effect causes cold, fresh groundwater to flow over salty and dense seawater, generating an SGD layer on the sea surface.

The temperature of the Mediterranean Sea oscillates seasonally between 26 - 30 ºC in summer and 14 - 19 ºC in winter, while the groundwater temperature remains relatively constant over time, implying a greater contrast between summer and winter. However, SGD spring visualizations in cloud-free images decrease significantly in winter months compared to warmer months (Figure 4). 35% of the springs were identified in summer and only 4% were identified in winter (Supplementary Material 4). Consequently, the number of SGD spring visualizations is much higher in summer than in winter. In winter months, wind, water column mixing, currents, etc., are more intense and reduce the thermal contrast. Therefore, environmental and marine conditions during the winter months are unfavorable for the identification of coastal springs.

For this reason, areas where the influence of various marine factors such as tides, coastal currents or fetch is small are ideal for identifying SGD springs, because such factors induce mixing attenuating the thermal contrast needed to identify SGD springs. Similarly, in subtropical areas such as the Mediterranean Sea, it is easier to identify SGD springs because coastal waters often develop a pycnocline during the summer months, resulting in less vertical mixing of the water column and therefore better identification of SGD springs. Therefore, in the Mediterranean basin, environmental and marine conditions in summer months are much more favorable for the identification of coastal springs than in winter months.

Eliminado: In the Mediterranean Sea, which has low tides and maximum thermal contrast between groundwater and seawater during summer and winter, the SGD spring visualizations in cloud-free images decrease significantly in winter months compared to warmer months (Figure 4). Only 2 of 21 SGD springs were identified during winter in 2017 (Anavalos Kiveri, Greece and Torre Badum, Spain) and 0 of 20 in 2018. The influence of marine factors in both cases was minimal; identification is therefore plausible during winter months. Since the number of SGD spring visualizations is much higher in summer than in winter, the environmental and marine conditions during winter months are unfavorable for the location of coastal springs.¶

Eliminado: Consequently, areas where the influence of various marine factors such as tides, coastal currents or fetch is small are ideal for identifying SGD springs, because such factors attenuate the thermal contrast needed to identify SGD springs. Similarly, in subtropical areas such as the Mediterranean Sea, it is easier to identify SGD springs because coastal waters often develop a pycnocline during the summer months, resulting in less vertical mixing of the water column and therefore better identification of SGD springs. Therefore, in the Mediterranean basin environmental and marine conditions in summer months are much more favorable for the identification of coastal springs than in winter months.¶

3.2.4 Coastal morphology limitation factors

Another aspect that influences SGD thermal plume visualization is the coastal morphology; depending on its characteristics, the seawater residence time in the study zone may allow the formation of a thermal plume. In semi-enclosed areas, such as bays or coves, where the residence time of discharging water in the sea is in the range of one to several days (Tamborski et al., 2020), the formation of thermal plumes from SGD can be easily be detected by satellite, in comparison with open sea areas, where the seawater residence time is shorter (less than a day), due to the effect of marine or weather factors such as waves, coastal currents or fetch. Groundwater discharge can occur below sea level, either at shallow (< 10 m) or at greater depths, right on the shoreline or a few meters from it (Zektser & Dzhamalov, 2006). The morphology of the coastal seabed combined with the geological characteristics of the aquifer (e.g., karstification degree and coastal hydraulic gradient) determine both the depth and offshore distance of the groundwater discharge. These two characteristics are very significant, since the location of the SGD spring on the coast is critical for the correct identification of the thermal contrast between groundwater and seawater using satellite thermal images. While groundwater discharges produced at coastal level or several meters inland usually generate thermal contrasts easily detectable by satellite (Mejías et al., 2012), submarine springs located several meters deep often represent a challenge for satellite detection. This is because when groundwater discharges below sea level, it rises to the sea surface generating a buoyant thermal layer of several millimeters, due to its lower density that arises from its temperature and salinity

Eliminado: or

Eliminado: These two characteristics are very important, since the SGD spring's location on the coast is critical to the correct formation of the plume and the thermal contrast between groundwater and seawater that must be recorded by satellite.

characteristics. Therefore, a greater discharge depth requires more time to reach the sea surface, adapting the SGD's thermal signal at the sea surface to the surrounding water temperature. Thus, marine factors may have a greater influence in balancing the seawater and groundwater temperatures, preventing the recognition of thermal anomalies on the sea surface, as stated by Mallast et al. (2013).

However, the time required for groundwater to reach the sea surface depends not only on the depth of the discharge below sea level, but also on hydrogeological factors, such as the discharge flow. Thus, SGD springs characterized by shallow depths and large flow rates will favor the detection of SGD-induced thermal plumes on the sea surface, while deep areas with small flows will be undetectable. Intermediate situations, such as shallow areas with small flows or deep areas with large flows, may be detected depending of the relative importance of the environmental and/or marine limiting factors.

For studied springs in the Mediterranean Sea basin, 52% of the springs were located in semi-enclosed coastal areas (Supplementary Material 4). Of these, 31% of the studied springs were identified (Port Miou and Bestouan in France; Cephalonia, Anavalos Kiveri and Almyros of Agios Nikolaos in Greece; Martinscica, Perilo, Novijanska, Jurjevska and Patan in Croatia; and Gokova (three springs), Ovacik and Antalya (three springs) in Turkey). These results show that when discharge occurs in semi-enclosed areas, where the seawater residence time is large, the springs can be identified until late autumn, even though the flow of groundwater is relatively small (0.75 $m^3 \cdot s^{-1}$ was reported for the Ovacik spring in Turkey). Therefore, the success in identifying SGD springs in semi-enclosed areas also is higher throughout the year.

Of the 54 SGD studied springs, the distance and depth information are available for 41% of the springs (Supplementary Material 4). The first group of springs, which discharge near the seashore and reach the sea through small streams, represents 6% of the springs (Patan in Croatia, Almyros of Iraklio in Greece and Maro in Spain) and from those, 66% were identified (Patan and Almyros of Iraklio). The second group of springs, which represent 6% (Font Dame, Font Estramar and Vise) characterized by discharge in coastal lagoons, was not identified. The third group of springs, which discharge close to the shoreline and in shallow water, represents 20% of the springs (Torre Badum, Las Fuentes, Font de Dins in Spain, Ain Zayana in Libya, Agios Nikolaos, Cephalonia and Anavalos Kiveri in Greece and Ovacik (3 springs) and Gokova in Turkey) and we were able to identify 91% (all of them except Ain Zayana spring). No springs were identified from the fourth group, which represents 6% of the springs (Moraig in Spain and Port Miou and Bestouan in France), and is characterized by discharge close to the shoreline but at a water column depth of 12 m.b.s.l. None of the springs of the fifth group (Mortola in Italy and Chekka in Lebanon), which represent 4% of the springs, characterized by discharge offshore with a water column depth between 35 and 150 m.b.s.l, were identified.

From the analysis of the images obtained by Landsat 8 TIRS and considering the hydrogeological data of the various coastal springs, we conclude that groundwater discharges that occur at significant depths (> 12 m.b.s.l) are unlikely be identified by this technique, probably because the thermal anomaly generated between groundwater and seawater does not reach the sea surface. This is the probable reason for the failure to identify the springs of Vise in France, Mortola in Italy and Chekka in Lebanon. For the Vise

Eliminado:

Eliminado: For the karstic springs studied in the Mediterranean Sea basin, 28 of the 54 springs studied were located in semi-enclosed coastal areas. Of these, 16 were identified by satellite. These springs were Port Miou and Bestouan in France; Cephalonia, Anavalos Kiveri and Almyros of Agios Nikolaos in Greece; Martinscica, Perilo, Novijanska, Jurjevska and Patan in Croatia; and Gokova (four springs), Ovacik and Antalya (four springs) in Turkey.

Eliminado: Our study showed that, of the 54 studied springs for which information is available, the seashore distances ranged from the shoreline to 1 km, and the discharge depths vary between 7 to -150 m with respect to sea level. The first group of springs discharge near the seashore and reach the sea through small streams; these karstic springs are located between 300 and 500 m inland and at elevations of 2 m, 3 m and 15 m above sea level for Patan in Croatia, Almyros of Iraklio in Greece and Maro in Spain, respectively. Of them, only Patan and Almyros of Iraklio were identified. The second group of springs discharges in coastal lagoons at a distance of 100 m from shore and a depth of -4 m (Font Dame and Font Estramar in Salses-Laucate lagoon in France) and an unknown shore distance and -30 m (Vise in Thau lagoon). None of these springs were identified. The third group of springs is located between 0 and 10 m from the shoreline and in shallow waters between 0 and -7 m (Torre Badum, Las Fuentes, Font de Dins in Spain, Ain Zayana in Libya, Agios Nikolaos, Cephalonia and Anavalos Kiveri in Greece and Ovacik and Gokova in Turkey). All of these springs were identified except the Ain Zayana spring in Libya.¶
The fourth group of springs is located close to the shoreline, but at a water column depth of -12 m. The two springs of this group were identified (Moraig in Spain and Port Miou and Bestouan in France). Neither of the two springs representing the fifth and last group, in which discharges occurs offshore between 100 m and 1 km with a water column depth between -35 and -150 m (Mortola in Italy and Chekka in Lebanon) were identified.¶

Eliminado: it is

spring, which discharges at 30 m.b.s.l, the hydrogeological information indicates that it is a mixture of karstic water, thermal water and seawater (Aquilina et al., 2002); most likely the discharging groundwater does not produce enough thermal contrast to be detected with a satellite sensor. On the other hand, SGD springs located in very shallow areas, such as the Salses-Laucate lagoon, which has an average maximum depth of 2 m.b.s.l (Bejannin et al., 2017), and where there are two well-known springs (Font Dame and Font Estramar) were not identified. A possible reason is that these types of shallow coastal lagoons are highly influenced by atmospheric temperature, since the small water column has little capacity to buffer temperature fluctuations (Lee et al., 2016). However, Anavalos Kiveri and Torre Badum, identified during winter months, are shallow (0 and to 10 m.b.s.l) SGD springs. Therefore, although initially these types of springs should be easily detectable by satellite, atmospheric factors can greatly influence the formation of the thermal contrast needed to identify them.

The shore distance at which groundwater discharge occurs is another factor that affects the identification of groundwater discharge in coastal areas. SGD springs discharging further than 500 m from the seashore were not recognized, such as the Mortola spring with a distance of 800 m. This may be related to the fact that as the distance to the coast increases, the depth of the water column increases, and the travel time of the fresher groundwater also increases, allowing a complete temperature equilibrium. Furthermore, these zones are more affected by ocean currents that increase water mixing, attenuating the thermal signal.

In some cases, there is no one single factor affecting SGD spring identification, but rather a combination of several factors (flow rate, season, coastal morphology, etc.) which makes it difficult to explain why an SGD spring was not identified.

3.2.5 Thermal anomalies from streams and anthropogenic sources

When looking for coastal thermal anomalies by using satellite TIR images, some anomalies can be detected that are not necessarily related to SGD. These anomalies can be from natural sources, such as rivers or streams, or civilian facilities such as ports, thermal power plants, fish farms or wastewater treatment plants. These thermal anomalies may misidentify or mask some SGD springs when discharge occurs in shallow areas with high seawater residence times.

For example, natural water sources, such as small rivers or streams, also produce a thermal signal at sea. As SGD, they may have a different temperature than seawater. This is the case for the small river near Split in Croatia (Supplementary Material 5), which produces a thermal anomaly that could be misinterpreted as an SGD spring. Furthermore, when SGD and rivers discharge at the same location, the thermal signal of SGD will be masked and/or modified by surface water discharge. In the case of civil facilities, the most common facilities that could be confused with SGD springs would be the discharges from wastewater treatment plants as they usually discharge water with a different thermal signal than the sea. For example, in the Hyperion Treatment Plant (HTP) and the Orange County Sanitation District (OCSD) wastewater diversion events in Southern California, where treated water discharge takes place at depth, it is possible to detect its thermal effect on the coastal waters (DiGiacomo et al., 2004) with SST differences of at least 0.5 ºC identifiable with TIR-RS (Gierach et al., 2017). Other examples of civilian

Eliminado: -
Eliminado: depth
Eliminado: -
Eliminado: -
Eliminado: t a
Eliminado: 3.2.5 Anthropogenic sources¶

facilities that can generate thermal signals and induce non-identification or masking of SGD springs, are power plants or ports In the case of the Mediterranean Sea basin, it was observed that facilities located along NE of the Iberian Peninsula, such as the Vandellós II nuclear power plant, the port of Barcelona, and the port of Benicarló, showed thermal anomalies similar to those produced by the SGD springs (Supplementary Material 5). These outflows can also mask and modify the SGD thermal signal of the plume when both outflows take place at the same location, such as the case of Peñíscola in Spain, where the SGD discharge takes place at the same location as the port (Supplementary Material 5).

3.3 Application of the multi-temporal SST series method

In some studied areas, there may be low thermal contrast that can prevent the identification of SGD springs. In these cases, it is possible to deepen the analysis of the images by using the multi-temporal SST series proposed by Mallast et al. (2014) in the Dead Sea, which that minimizes the effect of the previously-indicated limiting factors. Unlike single images, the multi-temporal SST series method allows several images and thus several points in time to be integrated, accentuating the small thermal anomalies for easy identification. An example of the usefulness of the multi-temporal SST series method is in the Serra d'Irta (Eastern Iberian Peninsula) (Mejías et al., 2012; Garcia-Solsona et al., 2010; Trezzi et al., 2016). At this site, Mejías et al. (2012) identified four large thermal anomalies (Torre Badum, Punta del Pebret and Les Fonts springs) that were not identified using Landsat 7, by using airborne thermal remote sensing. Using single images with Landsat 8 TIRS, only the Torre Badum spring was identified, compared with the four thermal anomalies identified by aerial thermal infrared images in 2012. The multi-temporal SST series method, which integrates 10 cloud free images from 2017 to 2018, enables the identification of Torre Badum and Les Fonts, 2 of the 4 springs identified in 2012 by Mejías et al. (2012) (Figure 5).

Although the multi-temporal SST series method is better for identifying SGD springs because thermal contrast is enhanced, this method did not enable SGD spring identification in other places where the single image method did not identify them. Furthermore, with multi-temporal SST series, the temporal morphological information, such as the shape and size of the discharge plume, is lost (Mallast et al., 2013). Conversely, single images allow the identification of morphological variations in the discharge plume and the temperature variations along that plume. Therefore, if the study objective is to identify SGD springs, the multi-temporal SST series method is the best option, but if the objective is to study the SGD plume variation, single images are better.

3.4 Identification of new SGD springs: challenges and recommendations for future SGD studies

One of the main objectives of this study is to demonstrate the great usefulness of satellite TIR imagery at local and regional scales, identifying SGD springs not previously described in the scientific literature. An example of this usefulness is the identification of 21 SGD springs undescribed in the bibliography along the Croatian coast using single images (Figure 6). This demonstrates that the analysis of single images obtained from Landsat 8 TIRS allows the identification of new SGD springs. Therefore, this economical technique is very useful in inaccessible areas (Gumma & Pavelic, 2013; Edet et al., 1998; Sander et al.,

Eliminado: There are some coastal outflows originated from anthropogenic sources may mask or modify the SGD thermal signal or even generate a similar thermal signal such as wastewater treatment outflows, fish farms, ports, power plants, among others. For example, wastewater treatment facilities discharge directly to the coastal waters in relatively shallow waters. Even when discharged at depth during periods with high stratification, it is possible to detect its thermal effect on the coastal waters due to buoyant plumes to surface (DiGiacomo et al., 2004) with SST differences of at least 0.5 ºC identifiable with TIR-RS (Gierach et al., 2017). In the case of inland aquaculture, pumped seawater temperature may be modified to reach optimal growth conditions for some species. For instance, water at 15ºC is used in European sea bass hatcheries (Navarro-Martín et al., 2009).¶

Eliminado: i

Eliminado: i

Eliminado: that were not identified using Landsat 7. Usin

Eliminado: g

Eliminado: i

Eliminado: Furthermore, with multi-temporal SST series, the temporal morphological information of the discharge plume is lost (Mallast et al., 2013).

Eliminado: of

Eliminado: e

Eliminado: ¶

Eliminado: 3.4 Identification of new SGD springs in the Mediterranean basin¶

1996). For this reason, in the design of SGD studies at both local and regional levels, it is recommended that the coastal water temperatures for thermal anomalies first be screened using the presented satellite based TIR-RS approach, as this will help narrow the sampling surveys. Although the study of the thermal images during a single year should be sufficient to identify potential coastal springs, it is highly advisable to analyze thermal images over several years, since there may be one or several factors (technical, marine, environmental, hydrogeological, etc.) that may alter the SGD thermal signal.

Although this study focused on the discharge of groundwater from springs located in karst aquifers, the study of satellite TIR-RS images could be extrapolated to other types of aquifers where the discharge is more diffused and where the proportion of meteoric water is lower. To identify thermal plumes, water discharging into the sea, whether of meteoric origin or marine circulation, must have acquired sufficient thermal contrast in the coastal aquifer before discharge. This thermal contrast can also occur in places where coastal aquifers are volcanic rocks or fractured granites, and even in sedimentary formations. However, in each case, the specific geological context (aquifer matrix, hydraulic parameter distribution, etc.) should be considered in the analysis.

Several studies have shown the possibility of quantifying SGD through the study of thermal plumes obtained by aircrafts (Tamborski et al., 2015; Danielescu et al., 2009; Mejías et al.,2012). By determining the thermal plume area, which is often directly related to the discharge volume, SGD may be quantitatively identified. However, there are several factors that can alter the thermal plume shape that could result in error. Furthermore, because the TIR-RS image only allows us to observe less than 1 mm of the sea surface, and thus prevents a determination of the volume beneath the thermal plume, the required information is missing. Moreover, quantification by means of images represents a major challenge, because satellite images (e.g., Landsat 8 TIRS) can only be obtained once every 16 days, and many factors can alter the shape of the plume independent of the actual discharge. Therefore, unless the discharge occurs in locations where the environmental and marine conditions are well-known, quantification by satellite images represents a major challenge that should be further investigated.

Although this study focused regionally on the Mediterranean Sea basin, it can be extrapolated to other parts of the world, in places where the SGD has sufficient thermal contrast when discharging into the sea. This technique has been successfully used in regional areas such as Ireland (Wilson & Rocha, 2012; McCaul et al., 2016) or the Laizhou Bay in China (Xing et al., 2016). However, in areas where the thermal contrast between the sea and the aquifer is low and/or temperature does not fluctuate during the year, such as in tropical zones, the use of satellite images represents a challenge that must be explored in detail. Furthermore, it is important to perform an initial study to attempt to identify the previously-described main factors that can limit SGD spring identification in the study area, to try to control/avoid these effects.

4. Conclusions

This study demonstrates that satellite remote sensing is a useful tool for the identification of coastal SGD springs in karst aquifers, both locally and regionally, by performing an initial screening of the coastal

Eliminado: One of the main objectives of this study is to demonstrate the great usefulness of satellite TIR imagery at local and regional scales, identifying SGD springs not previously described in the scientific literature. An example of this usefulness is the identification of 21 SGD springs undescribed in the bibliography along the Croatian coast using single images (Figure 6). This demonstrates that the analysis of single images obtained from Landsat 8 TIRS allows the identification of new SGD springs. Therefore, this economical technique is very useful in inaccessible areas (Gumma & Pavelic, 2013; Edet et al., 1998; Sander et al., 1996).¶

¶

3.5 Challenge and recommendations for future SGD studies and application in other areas¶

This study has shown the usefulness of satellite images for identifying coastal springs in limestone karstified aquifers, both locally and regionally. Therefore, in the design of SGD studies at both local and regional levels, it is recommended to first screen the coastal water temperatures for thermal anomalies using the presented satellite based TIR approach that will help narrow the sampling surveys. Although the study of the thermal images during a single year should be sufficient to identify potential coastal springs, it is highly advisable to analyze thermal images over several years, since there may be one or several factors (technical, marine, environmental, hydrogeological, etc.) that may alter the SGD thermal signal. ¶

¶

Although this study focused on the discharge of groundwater from springs located in karst aquifers, the study of satellite TIR images could be extrapolated to other types of aquifers where the discharge is more diffused and where the proportion of meteoric water is lower. To identify thermal plumes, water discharging into the sea, whether of meteoric origin or marine circulation, must have acquired sufficient thermal contrast in the coastal aquifer before discharge. This thermal contrast can also occur in places where coastal aquifers are volcanic rocks or fractured granites, and even in sedimentary formations. However, in each case, the specific geological context (aquifer matrix, hydraulic parameter distribution, etc.) should be considered in the analysis. ¶

¶

Several studies have shown the possibility of quantifying SGD through the study of thermal plumes obtained by aircrafts (Tamborski et al., 2015; Danielescu et al., 2009). By determining the thermal plume area, which is often directly related to the discharge volume, SGD may be quantitatively identified. However, there are several factors that can alter the thermal plume shape that could result in error. Furthermore, because the TIR image only allows a observation of the less than 1 mm of thermal contrast on the sea surface prevents, a determination of the volume beneath the thermal plume is missing. Moreover, quantification by means of images represents a major challenge because satellite images (e.g., Landsat 8 TIRS) can only be obtained once every 16 days, and many factors can alter the shape of the plume independent of the actual discharge. Therefore, unless the discharge occurs in locations where the environmental and marine conditions are well-controlled, quantification by satellite images represents a major challenge that should be further investigated.¶

¶

Although this study focused regionally on the Mediterranean Sea basin, it can be extrapolated to other parts of the world, in places where the SGD has sufficient thermal contrast when discharging into the sea. This technique has been successfully used in regional areas such as Ireland (Wilson & Rocha, 2012; McCaul et al., 2016) or the Laizhou Bay in China (Xing et al., 2016). However, in areas where ... [11]

water temperature images to identify possible thermal anomalies that can help narrow SGD study sampling surveys. However, this study highlights limiting factors that should be considered: (1) technical limitations, (2) geological/hydrogeological characteristics, (3) environmental and marine conditions and (4) coastal geomorphology.

In the karstic coastal aquifer of the Mediterranean Sea basin, the highest success percentage of SGD visualizations was during June, July, August and September. The main factor limiting the identification of SGD springs were clouds, which are far more abundant in winter months. The best geological and hydrogeological settings for identifying SGD springs are karst systems with well-developed karstification that are well-connected to the sea, as well as those systems with poorly-developed, but highly-fractured karstification. Environmental and marine conditions in the summer months are much more favorable for the identification of coastal springs than in the winter months. Semi-enclosed areas, where the seawater residence time is large, favor the identification of SGD springs throughout the year. Groundwater discharges that occurred at a depth of more than 12 m.b.s.l or in very shallow waters were not identified. Also, SGD springs that discharged further than 500 m from the seashore were not recognized.

Multi-temporal SST series are better for identifying SGD springs in coastal zones, but the information for changes in the discharge plume changes is lost, while single images are more suited to studying the morphological variations in the discharge plume and temperature variations along the plume.

Although this study focused regionally on the Mediterranean Sea basin, it can be extrapolated to other parts of the world and other aquifer types, in places where the SGD has sufficient thermal contrast when discharging into the sea and where the specific geological contexts (e.g., aquifer matrix and hydraulic parameters distribution) are considered. Long time series are better for identifying SGD spring areas, since there may be one or several factors (technical, marine, environmental, hydrogeological, etc.) that can alter the SGD's thermal signal. It is recommended to first screen the coastal water temperature images obtained by satellite to identify possible thermal anomalies that will help narrow the sampling surveys. This technique allows the identification and quantification of SGD springs in zones without hydrogeological information.

Data availability

All data are available from the corresponding author upon request.

Author contribution

SJC, AF and JGO contributed to design and implementation of the research, to the analysis of the results and writing of the paper.

Eliminado:

Eliminado: deeper

Eliminado: o

Competing interests

The authors declare that they have no conflict of interest.

Acknowledgements

This work was partly funded by the projects PID2019-110212RB-C22, CGL2016-77122-C2-1-R/2-R PID2019-110311RB-C21, PID2019-110311RB-C21 and the "Maria de Maeztu" programme for Units of Excellence (CEX2019-000940-M) of the Spanish Government and the project TerraMAr ACA210/18/00007 of the Catalan Water Agency. The authors want to thank the support of the Generalitat de Catalunya to GHS (2017 SGR 1485) and MERS (2018 SGR-1588) for additional funding. Authors want to acknowledge Francisco Carreño Conde from the Universidad Rey Juan Carlos for the initial discussions on the topic and Ulf Mallast from the Helmholtz Centre for Environmental Research- UFZ for the review of the manuscript. Albert Folch is a Serra Húnter Fellow.

References

Akawwi, E., Al-Zouabi, A., Kakish, M., Koehn, F. and Sauter, M.: Using thermal infrared imagery (TIR) for illustrating the submarine groundwater discharge into the eastern shoreline of the Dead Sea-Jordan, Am. J. Environ. Sci., 4(6), 693–700, doi:10.3844/ajessp.2008.693.700, 2008.

Alorda-Kleinglass, Ruiz-Mallén, I., Diego-Feliu, M., Rodellas, V. Bruach-Menchén, J.M. and Garcia-Orellana, J. :(accepted)The social implications of Submarine Groundwater Discharge from an Ecosystem Services perspective: A systematic review. Earth Science Reviews,2021.

Alorda-Kleinglass, A., Garcia-Orellana, J., Rodellas, V., Cerdà-Domènech, M., Tovar-Sánchez, A., Diego-Feliu, M., Trezzi, G., Sánchez-Quilez, D., Sanchez-Vidal, A. and Canals, M.: Remobilization of dissolved metals from a coastal mine tailing deposit driven by groundwater discharge and porewater exchange, Sci. Total Environ., 688, 1359–1372, doi:10.1016/j.scitotenv.2019.06.224, 2019.

Anderson, M. P.: Heat as a ground water tracer, Ground Water, 43(6), 951–968, doi:10.1111/j.1745-6584.2005.00052.x, 2005.

Andreo, B. and Carrasco, F.: Estudio hidrogeológico del entorno de la Cueva de Nerja., 1993.

Andrisoa, A., Lartaud, F., Rodellas, V., Neveu, I. and Stieglitz, T. C.: Enhanced Growth Rates of the Mediterranean Mussel in a Coastal Lagoon Driven by Groundwater Inflow, Front. Mar. Sci., 6(December), 1–14, doi:10.3389/fmars.2019.00753, 2019.

Con formato: Inglés (americano)
Eliminado: and
Con formato: Normal (Web)
Con formato: Inglés (americano)
Con formato: Justificado
Con formato: Inglés (americano)
Con formato: Justificado
Eliminado: ¶ ¶

Bakalowicz, M.: Karst groundwater: A challenge for new resources, Hydrogeol. J., 13(1), 148–160, doi:10.1007/s10040-004-0402-9, 2005.

Bakalowicz, M.: Karst and karst groundwater resources in the Mediterranean, Environ. Earth Sci., 74(1), 5–14, doi:10.1007/s12665-015-4239-4, 2015.

Bakalowicz, M.: Coastal Karst groundwater in the mediterranean: A resource to be preferably exploited onshore, not from Karst Submarine springs, Geosci., 8(7), doi:10.3390/geosciences8070258, 2018.

Barberá, J. A. and Andreo, B.: Hydrogeological processes in a fluviokarstic area inferred from the analysis of natural hydrogeochemical tracers. The case study of eastern Serranía de Ronda (S Spain), J. Hydrol., 523, 500–514, doi:10.1016/j.jhydrol.2015.01.080, 2015.

Barsi, J. A., Barker, J. L. and Schott, J. R.: An Atmospheric Correction Parameter Calculator for a Single Thermal Band Earth-Sensing Instrument, Int. Geosci. Remote Sens. Symp., 5(C), 3014–3016, doi:10.1109/igarss.2003.1294665, 2003.

Bejannin, S., van Beek, P., Stieglitz, T., Souhaut, M. and Tamborski, J.: Combining airborne thermal infrared images and radium isotopes to study submarine groundwater discharge along the French Mediterranean coastline, J. Hydrol. Reg. Stud., 13(February), 72–90, doi:10.1016/j.ejrh.2017.08.001, 2017.

Boehm, A. B., Shellenbarger, G. G. and Paytan, A.: Groundwater discharge: Potential association with fecal indicator bacteria in the surf zone, Environ. Sci. Technol., 38(13), 3558–3566, doi:10.1021/es035385a, 2004.

Brunner, P., Hendricks Franssen, H. J., Kgotlhang, L., Bauer-Gottwein, P. and Kinzelbach, W.: How can remote sensing contribute in groundwater modeling?, Hydrogeol. J., 15(1), 5–18, doi:10.1007/s10040-006-0127-z, 2007.

Burnett, W. C. and Dulaiova, H.: Estimating the dynamics of groundwater input into the coastal zone via continuous radon-222 measurements, J. Environ. Radioact., 69(1–2), 21–35, doi:10.1016/S0265-931X(03)00084-5, 2003.

Chander, G., Markham, B. L. and Helder, D. L.: Summary of current radiometric calibration coefficients for Landsat MSS, TM, ETM+, and EO-1 ALI sensors, Remote Sens. Environ., 113(5), 893–903, doi:10.1016/j.rse.2009.01.007, 2009.

Dale, R. K. and Miller, D. C.: Spatial and temporal patterns of salinity and temperature at an intertidal groundwater seep, Estuar. Coast. Shelf Sci., 72(1–2), 283–298, doi:10.1016/j.ecss.2006.10.024, 2007.

Eliminado: ¶

¶

Basterretxea, G., Tovar-Sanchez, A., Beck, A. J., Masqué, P., Bokuniewicz, H. J., Coffey, R., Duarte, C. M., Garcia-Orellana, J., Garcia-Solsona, E., Martinez-Ribes, L. and Vaquer-Sunyer, R.: Submarine groundwater discharge to the coastal environment of a Mediterranean island (Majorca, Spain): Ecosystem and biogeochemical significance, Ecosystems, 13(5), 629–643, doi:10.1007/s10021-010-9334-5, 2010.¶

¶

Bayari, C. S. and Kurttaş, T.: Coastal and submarine karstic discharges in the Gökova Bay, SW Turkey, Q. J. Eng. Geol. Hydrogeol., 35(4), 381–390, doi:10.1144/1470-9236/01034, 2002.¶

DiGiacomo, P. M., Washburn, L., Holt, B. and Jones, B. H.: Coastal pollution hazards in southern California observed by SAR imagery: Stormwater plumes, wastewater plumes, and natural hydrocarbon seeps, Mar. Pollut. Bull., 49(11–12), 1013–1024, doi:10.1016/j.marpolbul.2004.07.016, 2004.

Donlon, C. J., Minnett, P. J., Gentemann, C., Nightingale, T. J., Barton, I. J., Ward, B. and Murray, M. J.: Toward Improved Validation of Satellite Sea Surface Skin Temperature Measurements for Climate Research, J. Clim., 15, 353–369, doi:10.1175/1520-0442(2002)015<0353:TIVOSS>2.0.CO;2, 2002.

Edet, A. E., Okereke, C. S., Teme, S. C. and Esu, E. O.: Application of remote-sensing data to groundwater exploration: A case study of the Cross River State, southeastern Nigeria, Hydrogeol. J., 6(3), 394–404, doi:10.1007/s100400050162, 1998.

Fleury, P., Bakalowicz, M. and de Marsily, G.: Submarine springs and coastal karst aquifers: A review, J. Hydrol., 339(1–2), 79–92, doi:10.1016/j.jhydrol.2007.03.009, 2007.

Garcés, E., Basterretxea, G. and Tovar-Sánchez, A.: Changes in microbial communities in response to submarine groundwater input, Mar. Ecol. Prog. Ser., 438, 47–58, doi:10.3354/meps09311, 2011.

Garcia-Orellana, J., López-Castillo, E., Casacuberta, N., Rodellas, V., Masqué, P., Carmona-Catot, G., Vilarrasa, M. and García-Berthou, E.: Influence of submarine groundwater discharge on 210Po and 210Pb bioaccumulation in fish tissues, J. Environ. Radioact., 155–156, 46–54, doi:10.1016/j.jenvrad.2016.02.005, 2016.

Garcia-Orellana, J., Rodellas, V., Tamborski, J., Diego-Feliu, M., van Beek, P., Weinstein, Y., Charette, M., Alorda-Kleinglass, A., Michael, H. A., Stieglitz, T. and Scholten, J.: Radium isotopes as submarine groundwater discharge (SGD) tracers: Review and recommendations, Earth-Science Rev., 103681, doi:10.1016/j.earscirev.2021.103681, 2021.

Gerace, A. and Montanaro, M.: Remote Sensing of Environment Derivation and validation of the stray light correction algorithm for the thermal infrared sensor onboard Landsat 8, Remote Sens. Environ., 191, 246–257, doi:10.1016/j.rse.2017.01.029, 2017.

GROUP, M.: Observation of Formation of Deep Water in the Mediterranean Sea, 1969, Nature, 227(5262), 1037–1040, doi:10.1038/2271037a0, 1970.

Gumma, M. K. and Pavelic, P.: Mapping of groundwater potential zones across Ghana using remote sensing, geographic information systems, and spatial modeling, Environ. Monit. Assess., 185(4), 3561–3579, doi:10.1007/s10661-012-2810-y, 2013.

Kelly, J. L., Glenn, C. R. and Lucey, P. G.: High-resolution aerial infrared mapping of groundwater discharge to the coastal ocean, Limnol. Oceanogr. Methods, 11(MAY), 262–277, doi:10.4319/lom.2013.11.262, 2013.

Eliminado: ¶
Elhatip, H.: The use of hydrochemical techniques to estimate the discharge of Ovac1k submarine springs on the Mediterranean coast of Turkey, Environ. Geol., 43(6), 714–719, doi:10.1007/s00254-002-0668-y, 2003.¶

Con formato: Inglés (americano)

Con formato: Normal (Web)

Eliminado: ¶
Garcia-Solsona, E., Garcia-Orellana, J., Masqué, P., Garcés, E., Radakovitch, O., Mayer, A., Estradé, S. and Basterretxea, G.: An assessment of karstic submarine groundwater and associated nutrient discharge to a Mediterranean coastal area (Balearic Islands, Spain) using radium isotopes, Biogeochemistry, 97(2), 211–229, doi:10.1007/s10533-009-9368-y, 2010.¶
¶

Eliminado: ¶
Gierach, M. M., Holt, B., Trinh, R., Jack Pan, B. and Rains, C.: Satellite detection of wastewater diversion plumes in Southern California, Estuar. Coast. Shelf Sci., 186, 171–182, doi:10.1016/j.ecss.2016.10.012, 2017.¶

Krest, J. M., Moore, W. S., Gardner, L. R. and Morris, J. T.: Marsh nutrient export supplied by groundwater discharge: Evidence from radium measurements, Global Biogeochem. Cycles, 14(1), 167–176, doi:10.1029/1999GB001197, 2000.

Lee, E., Kang, K. M., Hyun, S. P., Lee, K. Y., Yoon, H., Kim, S. H., Kim, Y., Xu, Z., Kim, D. J., Koh, D. C. and Ha, K.: Submarine groundwater discharge revealed by aerial thermal infrared imagery: a case study on Jeju Island, Korea, Hydrol. Process., 30(19), 3494–3506, doi:10.1002/hyp.10868, 2016.

Luijendijk, E., Gleeson, T. and Moosdorf, N.: Fresh groundwater discharge insignificant for the world's oceans but important for coastal ecosystems, Nat. Commun., 11(1), 1260, doi:10.1038/s41467-020-15064-8, 2020.

Mallast, U., Gloaguen, R., Friesen, J., Rödiger, T., Geyer, S., Merz, R. and Siebert, C.: How to identify groundwater-caused thermal anomalies in lakes based on multi-temporal satellite data in semi-arid regions, Hydrol. Earth Syst. Sci., 18(7), 2773–2787, doi:10.5194/hess-18-2773-2014, 2014.

McCaul, M., Barland, J., Cleary, J., Cahalane, C., McCarthy, T. and Diamond, D.: Combining remote temperature sensing with in-situ sensing to track marine/freshwater mixing dynamics, Sensors (Switzerland), 16(9), doi:10.3390/s16091402, 2016.

Mejías, M., Ballesteros, B. J., Antón-Pacheco, C., Domínguez, J. A., Garcia-Orellana, J., Garcia-Solsona, E. and Masqué, P.: Methodological study of submarine groundwater discharge from a karstic aquifer in the Western Mediterranean Sea, J. Hydrol., 464–465, 27–40, doi:10.1016/j.jhydrol.2012.06.020, 2012.

Michael, H. A., Mulligan, A. E. and Harvey, C. F.: Seasonal oscillations in water exchange between aquifers and the coastal ocean, Nature, 436(7054), 1145–1148, doi:10.1038/nature03935, 2005.

Moore, W. S.: The Effect of Submarine Groundwater Discharge on the Ocean, Ann. Rev. Mar. Sci., 2(1), 59–88, doi:10.1146/annurev-marine-120308-081019, 2010.

Moosdorf, N. and Oehler, T.: Societal use of fresh submarine groundwater discharge: An overlooked water resource, Earth-Science Rev., 171(August 2016), 338–348, doi:10.1016/j.earscirev.2017.06.006, 2017.

Moosdorf, N., Böttcher, M. E., Adyasari, D., Erkul, E., Gilfedder, B. S., Greskowiak, J., Jenner, A.-K., Kotwicki, L., Massmann, G., Müller-Petke, M., Oehler, T., Post, V., Prien, R., Scholten, J., Siemon, B., Ehlert von Ahn, C. M., Walther, M., Waska, H., Wunderlich, T. and Mallast, U.: A State-Of-The-Art Perspective on the Characterization of Subterranean Estuaries at the Regional Scale, Front. Earth Sci., 9, 95, doi:10.3389/feart.2021.601293, 2021.

Con formato: Inglés (americano)

Con formato: Justificado

Eliminado: ¶

Rocha, C., Robinson, C. E., Santos, I. R., Waska, H., Michael, H. A. and Bokuniewicz, H. J.: A place for subterranean estuaries in the coastal zone, Estuar. Coast. Shelf Sci., 250, 107167, doi:10.1016/j.ecss.2021.107167, 2021.

Rodellas, V., Garcia-Orellana, J., Garcia-Solsona, E., Masqué, P., Domínguez, J. A., Ballesteros, B. J., Mejías, M. and Zarroca, M.: Quantifying groundwater discharge from different sources into a Mediterranean wetland by using 222Rn and Ra isotopes, J. Hydrol., 466–467, 11–22, doi:10.1016/j.jhydrol.2012.07.005, 2012.

Rodellas, V., Garcia-Orellana, J., Masqué, P., Feldman, M., Weinstein, Y. and Boyle, E. A.: Submarine groundwater discharge as a major source of nutrients to the Mediterranean Sea, Proc. Natl. Acad. Sci. U. S. A., 112(13), 3926–3930, doi:10.1073/pnas.1419049112, 2015.

Rosenberry, D. O., Duque, C. and Lee, D. R.: History and evolution of seepage meters for quantifying flow between groundwater and surface water: Part 1 – Freshwater settings, Earth-Science Rev., 204, 103167, doi:10.1016/j.earscirev.2020.103167, 2020.

Rufí-Salís, M., Garcia-Orellana, J., Cantero, G., Castillo, J., Hierro, A., Rieradevall, J. and Bach, J.: Influence of land use changes on submarine groundwater discharge, Environ. Res. Commun., 1(3), 031005, doi:10.1088/2515-7620/ab1695, 2019.

Ruiz-González, C., Rodellas, V. and Garcia-Orellana, J.: The microbial dimension of submarine groundwater discharge: current challenges and future directions, FEMS Microbiol. Rev., doi:10.1093/femsre/fuab010, 2021.

Schubert, M., Scholten, J., Schmidt, A., Comanducci, J. F., Pham, M. K., Mallast, U. and Knoeller, K.: Submarine groundwater discharge at a single spot location: Evaluation of different detection approaches, Water (Switzerland), 6(3), 584–601, doi:10.3390/w6030584, 2014.

Shaban, A., Khawlie, M., Abdallah, C. and Faour, G.: Geologic controls of submarine groundwater discharge: Application of remote sensing to north Lebanon, Environ. Geol., 47(4), 512–522, doi:10.1007/s00254-004-1172-3, 2005.

Tamborski, J., van Beek, P., Conan, P., Pujo-Pay, M., Odobel, C., Ghiglione, J. F., Seidel, J. L., Arfib, B., Diego-Feliu, M., Garcia-Orellana, J., Szafran, A. and Souhaut, M.: Submarine karstic springs as a source of nutrients and bioactive trace metals for the oligotrophic Northwest Mediterranean Sea, Sci. Total Environ., 732, 1–14, doi:10.1016/j.scitotenv.2020.139106, 2020.

Taniguchi, M., Dulai, H., Burnett, K. M., Santos, I. R., Sugimoto, R., Stieglitz, T., Kim, G., Moosdorf, N. and Burnett, W. C.: Submarine Groundwater Discharge: Updates on Its Measurement Techniques, Geophysical Drivers, Magnitudes, and Effects, Front. Environ. Sci., 7(October), 1–26, doi:10.3389/fenvs.2019.00141, 2019.

Con formato: Inglés (americano)

Con formato: Inglés (americano)

Eliminado: ¶
Navarro-Martín, L., Blázquez, M., Viñas, J., Joly, S. and Piferrer, F.: Balancing the effects of rearing at low temperature during early development on sex ratios, growth and maturation in the European sea bass (Dicentrarchus labrax). Limitations and opportunities for the production of highly female-biased stocks, Aquaculture, 296(3–4), 347–358, doi:10.1016/j.aquaculture.2009.07.022, 2009.¶
¶
Povinec, P. P., Aggarwal, P. K., Aureli, A., Burnett, W. C., Kontar, E. A., Kulkarni, K. M., Moore, W. S., Rajar, R., Taniguchi, M., Comanducci, J. F., Cusimano, G., Dulaiova, H., Gatto, L., Groening, M., Hauser, S., Levy-Palomo, I., Oregioni, B., Ozorovich, Y. R., Privitera, A. M. G. and Schiavo, M. A.: Characterisation of submarine groundwater discharge offshore south-eastern Sicily, J. Environ. Radioact., 89(1), 81–101, doi:10.1016/j.jenvrad.2006.03.008, 2006.¶
¶

Con formato: Inglés (americano)

Con formato: Justificado

Eliminado: ¶
¶

Con formato: Inglés (americano)

Con formato: Justificado

Eliminado: ¶
¶

Tcherepanov, E. N., Zlotnik, V. A. and Henebry, G. M.: Using Landsat thermal imagery and GIS for identification of groundwater discharge into shallow groundwater-dominated lakes, Int. J. Remote Sens., 26(17), 3649–3661, doi:10.1080/01431160500177315, 2005.

Trezzi, G., Garcia-Orellana, J., Rodellas, V., Santos-Echeandia, J., Tovar-Sánchez, A., Garcia-Solsona, E. and Maqué, P.: Submarine groundwater discharge: a significant source of dissolved trace metals to the North Western Mediterranean Sea. Marine Chemistry, Mar. Chem., 186, 90–100, doi:10.1016/j.marchem.2016.08.004, 2016.

Trezzi, G., Garcia-Orellana, J., Rodellas, V., Masqué, P., Garcia-Solsona, E. and Andersson, P. S.: Assessing the role of submarine groundwater discharge as a source of Sr to the Mediterranean Sea, Geochim. Cosmochim. Acta, 200, 42–54, doi:10.1016/j.gca.2016.12.005, 2017.

Tulipano, L., Panagopoulus, A. and Fidelibus, M. D.: COST ACTION 621"Groundwater management of coastal karstic aquifers",Final Report., 2005.

Varma, S., Turner, J. and Underschultz, J.: Estimation of submarine groundwater discharge into Geographe Bay, Bunbury, Western Australia, J. Geochemical Explor., 106(1–3), 197–210, doi:10.1016/j.gexplo.2010.02.003, 2010.

Wang, L. T., McKenna, T. E. and Deliberty, T. L.: Locating Ground-Water Discharge Areas In Rehoboth And Indian River Bays And Indian River, Delaware Using Landsat 7 Imagery., 2008.

Werner, A. D., Bakker, M., Post, V. E. A., Vandenbohede, A., Lu, C., Ataie-Ashtiani, B., Simmons, C. T. and Barry, D. A.: Seawater intrusion processes, investigation and management: Recent advances and future challenges, Adv. Water Resour., 51, 3–26, doi:10.1016/j.advwatres.2012.03.004, 2013.

Wilson, J. and Rocha, C.: Regional scale assessment of Submarine Groundwater Discharge in Ireland combining medium resolution satellite imagery and geochemical tracing techniques, Remote Sens. Environ., 119, 21–34, doi:10.1016/j.rse.2011.11.018, 2012.

Wloczyk, C., Richter, R., Borg, E. and Nueberts, W.: Sea and lake surface temperature retrieval from Landsat thermal data in Northern Germany, Int. J. Remote Sens., 27 (12), 2489–2502, doi:10.1080/01431160500300206, 2006.

Worthington, S. R. H.: A comprehensive strategy for understanding flow in carbonate aquifers, Karst Model., 30–37, 1999.

Wulder, M. A., Loveland, T. R., Roy, D. P., Crawford, C. J., Masek, J. G., Woodcock, C. E., Allen, R. G., Anderson, M. C., Belward, A. S., Cohen, W. B., Dwyer, J., Erb, A., Gao, F., Griffiths, P., Helder, D., Hermosilla, T., Hipple, J. D., Hostert, P., Hughes, M. J., Huntington, J., Johnson, D. M., Kennedy, R.,

Eliminado: ¶
Wen-Yao, L., Field, R. T., Gantt, R. G. and Klemas, V.: Measurement of the Surface Emissivity, Remote Sens. Environ., 5(4), 97–109, doi:10.1016/0034-4257(87)90009-5, 1987.¶

Kilic, A., Li, Z., Lymburner, L., McCorkel, J., Pahlevan, N., Scambos, T. A., Schaaf, C., Schott, J. R., Sheng, Y., Storey, J., Vermote, E., Vogelmann, J., White, J. C., Wynne, R. H. and Zhu, Z.: Current status of Landsat program, science, and applications, Remote Sens. Environ., 225(February), 127–147, doi:10.1016/j.rse.2019.02.015, 2019.

Xing, Q., Braga, F., Tosi, L., Lou, M., Zaggia, L., Teatini, P., Gao, X., Yu, L., Wen, X. and Shi, P.: Detection of Low Salinity Groundwater Seeping into the Eastern Laizhou Bay (China) with the Aid of Landsat Thermal Data, J. Coast. Res., 74, 149–156, doi:10.2112/si74-014.1, 2016.

Zektser, I. S., Everett, L. G. and Dzhamalov, R. G.: Submarine Groundwater., 2006.

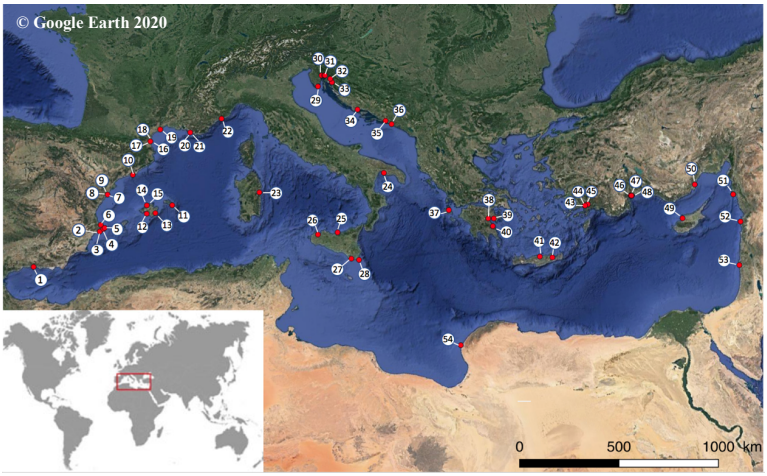

Figure 1. Location of the 54 SGD springs used for this study. SGD spring shown in the figure are described in Bakalowicz, 2018; Basterretxea et al., 2010; Fleury et al., 2007; Garcia-Solsona etal ., 2010 and Mejías et al., 2012. © Google Earth 2020.

Tabla con formato

Eliminado: Figure 1. Location of the 54 SGD springs used for this study. SGD spring shown in the figure are described in Bakalowicz, 2018; Basterretxea et al., 2010; Fleury et al., 2007 and Mejías et al., 2012. ¶

... [12]

Eliminado: Figure 2. SST images (ºC) obtained with Band 10 of Landsat 8 OLI/TIRS of the region of Almyros of Agios Nikolaos (Greece) along 2017. Of the 23 images analyzed, the presence of a SGD spring was clearly visible in 9 images that represents a 37.5% of success. In January and November 2017, it was not possible to obtain a SST image due to the presence of clouds. Negative values in dark blue represent clouds. © Google Earth 2020¶

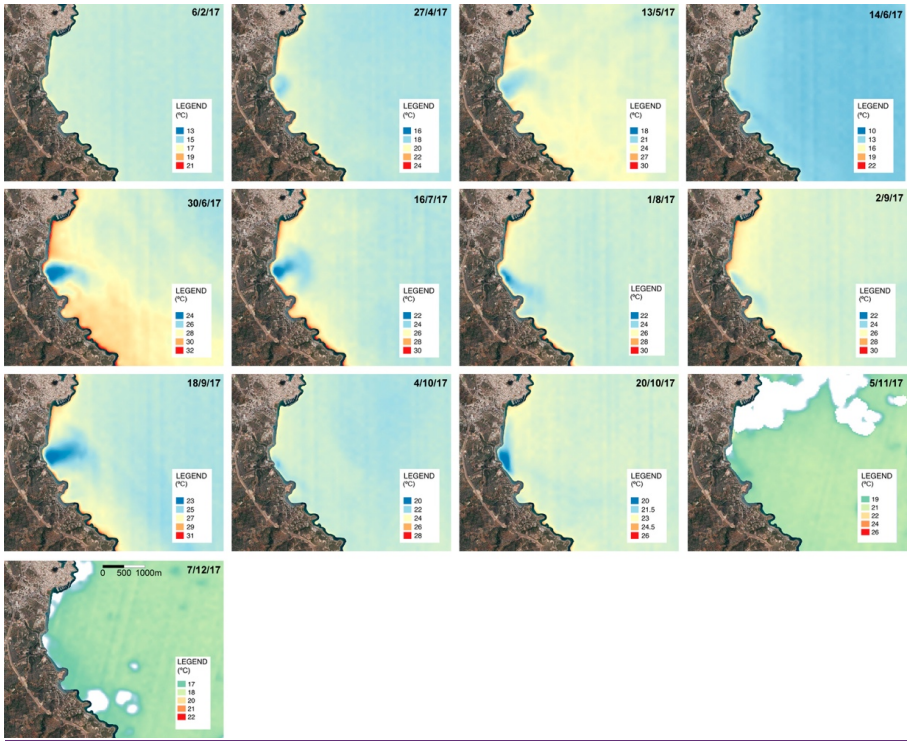

Figure 2. SST images (°C) obtained via Band 10 of Landsat 8 OLI/TIRS of the region of Almyros of Agios Nikolaos (Crete, Greece) throughout 2017. Of the 23 images analyzed, the presence of an SGD spring was clearly visible in 9 images that represents a 37% ratio of success. In January, March and November 2017, it was not possible to obtain an SST image due to the presence of clouds. © Google Earth 2020.

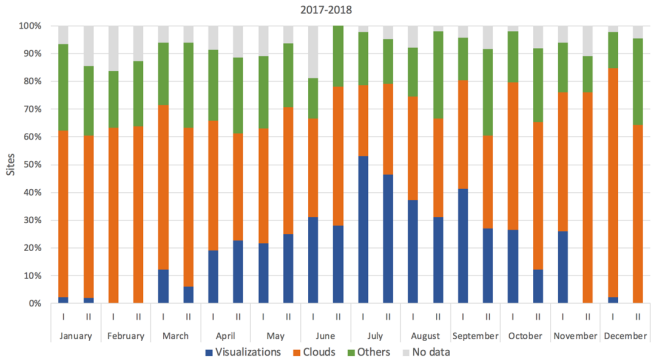

Figure 3. Percentage of successful and unsuccessful SGD identifications for all SGD springs that were identified at least once (23 springs representing 44%) throughout the year 2017 and during the year 2018 (based on the selection of 720 images), are shown individually in the Supplementary Material 3. Percentage of successful and unsuccessful SGD identifications for all SGD springs that were identified at least once throughout 2017 and 2018, are in Supplementary Material 3. The X-axis shows the months of the year. Roman numerals (I and II) represent the two satellite passes per month that cover every area. No image available is represented in grey, color while the presence of clouds is in orange and blue for successful SGD identifications. Those in which images were not covered by clouds, but SGD springs were not identified, are shown in the figure as "others" in green color.

Con formato: Punto de tabulación: 0,33 cm, Izquierda

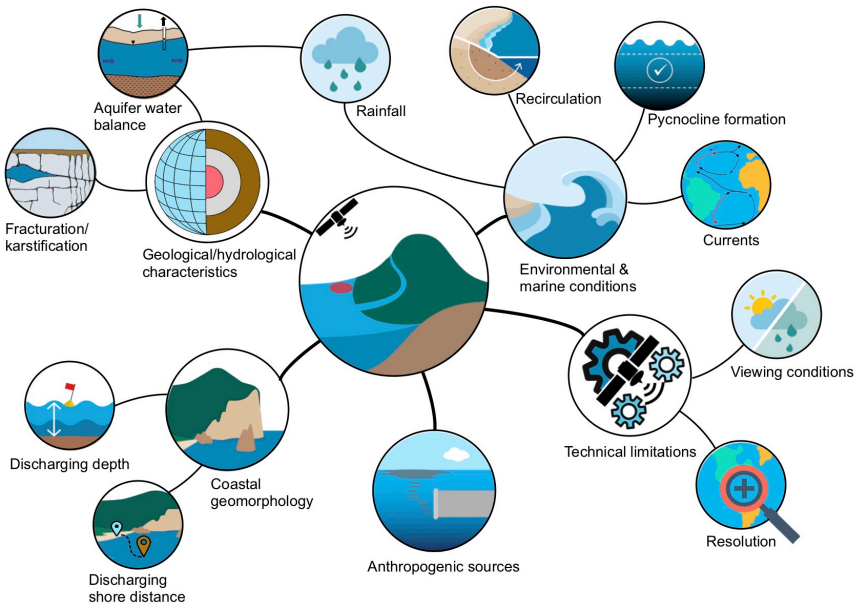

Figure 4. Conceptual framework of technical limitation factors that can limit the identification of SGD springs by using Landsat 8 TIRS images.

Con formato: Fuente: 9 pto, Negrita

Con formato: Izquierda

Con formato: Izquierda

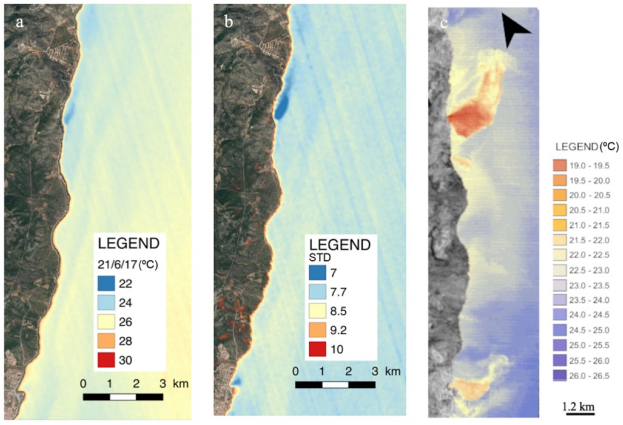

Figure 5. a) Serra d'Irta single image map using an image taken on 21/6/17. One spring in the middle of the Torre Badum spring was identified. b) Serra d'Irta Standard Deviation (STD) map using 10 cloud free images acquired between 2017-2018. Two springs in Serra d'Irta, in the south the Les Fonts beach in Alcossebre spring, and in the middle the Torre Badum spring, were identified. c) Image modified from Mejías et al. (2012) where SGD springs were identified using aerial thermal infrared images.

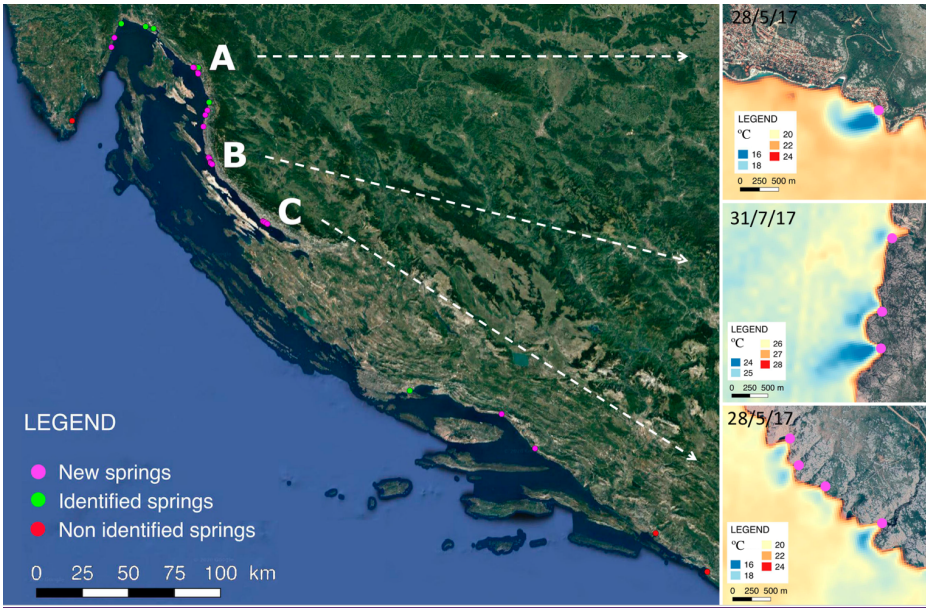

Figure 6. Springs reported in the literature (described SGD spring) vs new SGD spring identified with Landsat 8 TIRS. New SGD springs, not reported in the literature are represented in pink. Springs reported in the literature are represented in white.

Eliminado: <object><object><object><object><object>

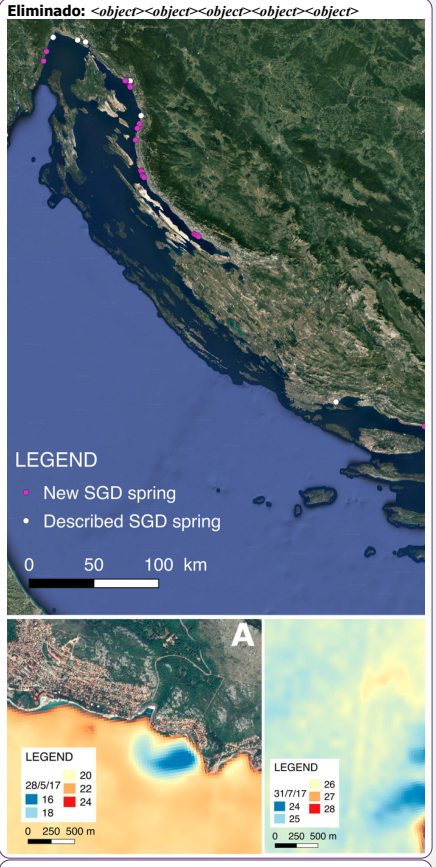

Eliminado: Figure 6. Springs reported in the literature (described SGD spring) vs new SGD spring identified with Landsat 8 TIRS. New SGD springs, not reported in the literature are represented with pink colour. Springs reported in the literature are represented with white colour.

Página 7: [1] Con formato	**Usuario de Microsoft Office**	**3/6/21 10:09:00**

Inglés (americano)

Página 7: [1] Con formato	**Usuario de Microsoft Office**	**3/6/21 10:09:00**

Inglés (americano)

Página 7: [2] Con formato	**Usuario de Microsoft Office**	**3/6/21 10:09:00**

Inglés (americano)

Página 7: [2] Con formato	**Usuario de Microsoft Office**	**3/6/21 10:09:00**

Inglés (americano)

Página 7: [3] Con formato	**Usuario de Microsoft Office**	**3/6/21 10:09:00**

Inglés (americano)

Página 7: [3] Con formato	**Usuario de Microsoft Office**	**3/6/21 10:09:00**

Inglés (americano)

Página 7: [3] Con formato	**Usuario de Microsoft Office**	**3/6/21 10:09:00**

Inglés (americano)

Página 7: [4] Con formato	**Usuario de Microsoft Office**	**3/6/21 10:09:00**

Inglés (americano)

Página 7: [4] Con formato	**Usuario de Microsoft Office**	**3/6/21 10:09:00**

Inglés (americano)

Página 7: [4] Con formato	**Usuario de Microsoft Office**	**3/6/21 10:09:00**

Inglés (americano)

Página 7: [4] Con formato	**Usuario de Microsoft Office**	**3/6/21 10:09:00**

Inglés (americano)

Página 7: [5] Con formato	**Usuario de Microsoft Office**	**3/6/21 10:11:00**

Inglés (americano)

Página 7: [5] Con formato	**Usuario de Microsoft Office**	**3/6/21 10:11:00**

Inglés (americano)

Página 7: [6] Con formato	**Usuario de Microsoft Office**	**3/6/21 10:11:00**

Inglés (americano)

Página 7: [6] Con formato	**Usuario de Microsoft Office**	**3/6/21 10:11:00**

Inglés (americano)

Página 7: [7] Con formato	**Usuario de Microsoft Office**	**3/6/21 10:14:00**

Inglés (americano)

Página 7: [7] Con formato	**Usuario de Microsoft Office**	**3/6/21 10:14:00**

Inglés (americano)

Página 7: [8] Con formato	**Usuario de Microsoft Office**	**3/6/21 10:11:00**

Fuente: TimesNewRomanPSMT, Inglés (americano)

Página 7: [8] Con formato	**Usuario de Microsoft Office**	**3/6/21 10:11:00**

Fuente: TimesNewRomanPSMT, Inglés (americano)

Página 7: [8] Con formato	**Usuario de Microsoft Office**	**3/6/21 10:11:00**

Fuente: TimesNewRomanPSMT, Inglés (americano)

Página 7: [8] Con formato	**Usuario de Microsoft Office**	**3/6/21 10:11:00**

Fuente: TimesNewRomanPSMT, Inglés (americano)

Página 7: [9] Eliminado	**Usuario de Microsoft Office**	**3/6/21 11:15:00**

Página 7: [9] Eliminado	**Usuario de Microsoft Office**	**3/6/21 11:15:00**

Página 7: [10] Con formato	**Usuario de Microsoft Office**	**3/6/21 10:14:00**

Inglés (americano)

Página 7: [10] Con formato	**Usuario de Microsoft Office**	**3/6/21 10:14:00**

Inglés (americano)

Página 16: [11] Eliminado	**Usuario de Microsoft Office**	**3/6/21 9:17:00**

Página 24: [12] Eliminado	**Usuario de Microsoft Office**	**3/6/21 9:20:00**